UNIVERSITY OF AMSTERDAM

UvA-DARE (Digital Academic Repository)

Coding cognition

Representing and communicating information in perceptual and memory systems

Dorman, R.

Publication date
2025

Link to publication

Citation for published version (APA):
Dorman, R. (2025). *Coding cognition: Representing and communicating information in perceptual and memory systems*. [Thesis, fully internal, Universiteit van Amsterdam].

General rights
It is not permitted to download or to forward/distribute the text or part of it without the consent of the author(s) and/or copyright holder(s), other than for strictly personal, individual use, unless the work is under an open content license (like Creative Commons).

Disclaimer/Complaints regulations
If you believe that digital publication of certain material infringes any of your rights or (privacy) interests, please let the Library know, stating your reasons. In case of a legitimate complaint, the Library will make the material inaccessible and/or remove it from the website. Please Ask the Library: https://uba.uva.nl/en/contact, or a letter to: Library of the University of Amsterdam, Secretariat, P.O. Box 19185, 1000 GD Amsterdam, The Netherlands. You will be contacted as soon as possible.

UvA-DARE is a service provided by the library of the University of Amsterdam (https://dare.uva.nl)

Download date:08 Nov 2026

Chapter 2

Spiked-based coupling between single neurons and populations across rat sensory cortices, perirhinal cortex and hippocampus

R. Dorman, J. Bos, M.A. Vinck, J.A.M. Lorteije, I. Reiten, J. G. Bjaalie, J. Fiorilli, M. Okun, C.M.A. Pennartz

Published in *Cerebral Cortex,* 2023
doi: 10.109/cercor/bhad111

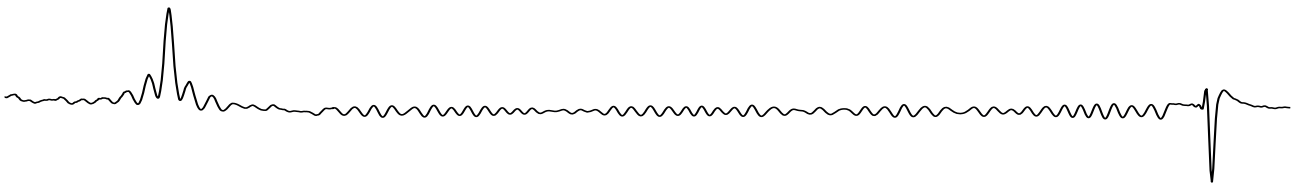

2.1 Abstract

Cortical computations require coordination of neuronal activity within and across multiple areas. We characterized spiking relationships within and between areas by quantifying coupling of single neurons to population firing patterns. Single-neuron population coupling (SNPC) was investigated using ensemble recordings from hippocampal CA1 region and somatosensory, visual and perirhinal cortices. Within-area coupling was heterogeneous across structures, with area CA1 showing higher levels than neocortical regions. In contrast to known anatomical connectivity, between-area coupling showed strong firing coherence of sensory neocortices with CA1, but less with perirhinal cortex. Cells in sensory neocortices and CA1 showed positive correlations between within-area and between-area coupling; these were weaker for perirhinal cortex. All four areas harboured broadcasting cells, connecting to multiple external areas, which was uncorrelated to within-area coupling strength. When examining correlations between SNPC and spatial coding we found that, if such correlations were significant, they were negative. This result was consistent with an overall preservation of SNPC across different brain states, suggesting a strong dependence on intrinsic network connectivity. Overall, SNPC offers an important window on cell-to-population synchronization in multi-area networks. Instead of pointing to specific information-coding functions, our results indicate a primary function of SNPC in dynamically organizing communication in cross-areal systems.

Keywords: Brain state, multi-area networks, network dynamics, population coupling, spatial selectivity,

2.2 Introduction

Computations in the mammalian brain require coordinated activity of networks of interconnected neurons (Barthó et al., 2004; DeCharms & Zador, 2000; Harris et al., 2003; Perich & Rajan, 2020; Yuste, 2015). For example, computations underlying the transformation of sensory information into episodic memory and subsequent memory retrieval are thought to require bidirectional communication between cortical sensory areas and (para)hippocampal areas (Eichenbaum, 2000; Squire & Zola-Morgan, 1991; Whittington et al., 2020). Such multi-area networks composed of local networks have been dubbed 'meta-networks' to denote the requirement for a higher order of integration across the brain than can be achieved within single structures such as primary visual cortex (Pennartz, 2015). These networks are subject to anatomical and physiological constraints, such as decreasing likelihood of having connectivity with increasing distance (Ercsey-Ravasz et al., 2013; Wang & Kennedy, 2016). While brain-wide networks have been investigated with anatomical methods (e.g. Harris et al., 2019), functional connectivity need not align with anatomy per se. A method to assess meta-network characteristics of neural networks is to consider the functional relationships between spiking activity of single neurons and entire populations, quantified by crosscorrelating single unit and population spiking activity (Okun et al., 2015). The strength of this Single Neuron-Population Coupling (SNPC) reflects the relationship between activity of the reference cell and the population's dynamics.

Here, we examined multi-area network dynamics by assessing SNPC within and between four distinct cortical areas in freely moving rats performing a figure-8 maze task, as well as during quiet wakefulness and non-REM sleep. To study population coupling along the sensory-to-hippocampal hierarchy, we recorded cells from primary visual cortex (V1), the barrel field of primary somatosensory cortex (S1BF), hippocampal area CA1 and perirhinal cortex (PER). While strong SNPC within a single cortical area has been reported (Bachatene et al., 2015; Okun et al., 2015, 2019), we predict this to be markedly less strong and less temporally precise between different brain structures, depending on anatomical and physiological constraints such as distance (cf. Wang & Kennedy, 2016; (Clancy et al., 2019). Furthermore, we expect functional and anatomical relationships between areas to be reflected in the SNPC. For instance, previous data indicate that primary sensory areas have modest levels of directnterconnectivity (Meijer et al., 2017; Zakiewicz et al., 2014, Iurilli et al., 2012). Sensory inputs are known to reach the hippocampus indirectly via the perirhinal and postrhinal cortex (Agster & Burwell, 2009; Burwell, Rebecca & Amaral, David, 1998; Naber et al., 1999, 2000; Zakiewicz et al., 2014), but not directly - which predicts stronger coupling from sensory cortices to PER than to hippocampus. Lastly, we expect putative Fast Spiking (FS) interneurons to be coupled mainly locally.

The availability of both within- and between-area SNPC data also raises the question how these two forms of coupling are related (Clancy et al., 2019). In other words, are there 'hub' or 'broadcasting' cells that do not only display local synchrony, but also regulate dynamics and information-processing in distant populations (Stevens & Zador, 1998)?

An alternative configuration holds that individual neurons mediate only one type of coupling, so that some engage strongly only in local interactions, whereas others couple strongly to external, but not local populations. Multi-area SNPC analysis allowed us to investigate whether single cells are specifically coupled to only one target area or show a broadcasting configuration where each neuron couples to multiple areas, which may support a role of single neurons in meta-network functioning. We hypothesize that a higher degree of external broadcasting of a cell coincides with strong local synchrony.

SNPC may be governed by hard-wired connectivity and internal systems dynamics (Okun et al., 2015), but possibly also by behavioural factors, such as the subject's navigation through space and the correlative dynamics arising from hippocampal cells having nearby place fields (O'Keefe & Dostrovsky, 1971). Thus, we investigated whether SNPC correlates with spatial coding by CA1 and neocortical cells. Furthermore, If SNPC values primarily depend on behavioural variables, one would not expect SNPC relationships to be conserved across different brain states. If, in contrast, SNPC is governed by hard-wired connectivity and intrinsic dynamics, we would expect SNPC and levels of broadcasting to remain similar across brain states.

In summary, we address four questions on SNPC within and across sensory cortical and (para)hippocampal areas: (i) How does single-neuron-to-population coupling within and between areas differ across various cortical areas, and does this follow known anatomical and functional constraints? (ii) Are levels of within and between-area population coupling correlated? (iii) Are there neurons that couple strongly to populations in multiple areas? (iv) Is SNPC mediated by fixed, intrinsic properties or is it governed by the dynamics associated with behavioural activity and concomitant spatial coding?

2.3 Materials and Methods

Behavioural apparatus and task

All experiments were conducted in accordance with the National Guidelines on Animal Experiments and were approved by the Animal Experimentation Committee of the University of Amsterdam. Details of the experiment were previously described in Bos et al. (2017). Briefly, food restricted rats (N=3, same individuals as in Bos et al., 2017) were trained to perform a two-choice visual discrimination task on a figure-eight maze (fig. 1a, b). The animal was confined to the middle arm until a tone indicated a trial could be started by approaching the front barrier in the middle arm and breaking a photobeam, placed just before the front barrier. This triggered the onset of a visual stimulus on two monitors at the end of the middle arm with a 1 second delay. Visual stimuli (two equiluminant wingding-font symbols; a plane and a diamond) were presented on two monitors placed in front of the initial arm segments of the maze; one of the monitors displayed a CS+ stimulus and the other one the CS- stimulus. Which monitor displayed the CS+ or CS- changed from trial to trial in a manner unpredictable to the rat. Visual stimuli were presented until the animal ventured in either the right or left arm and passed a 'point of no return'. Part of each arm was covered with sandpaper to provide tactile stimulation, and the coarseness of the texture was associated with the size of the reward in case of a correct trial. When the rat chose to enter the arm corresponding to the CS+ location, it received a food reward at the end of that arm. Choosing the arm marked by the CS- did not result in reward. Upon returning to the middle arm another, an additional smaller food reward was delivered. Animal position was estimated with photobeams at several points on the maze, as well as with an overhead video-camera. Additional details have been described in (Vinck et al., 2016; Bos et al., 2017).

Electrophysiological data acquisition

We performed simultaneous tetrode recordings in S1BF, V1, PER and CA1. These areas are of interest because rats are highly skilled in using tactile abilities while exploring their environment; the visual modality had to be used to make correct choices in the task; the hippocampus is involved in spatial representations and memory, and PER is situated as a higher-level, multimodal cortical area with direct and indirect connections to the hippocampal region. After behavioural training, the animals were implanted with a custom-made microdrive ('quaddrive'; Technology Center, Faculty of Science, University of Amsterdam), consisting of 32 tetrodes, split equally over four areas: V1, S1BF, hippocampal area CA1 and PER (fig. 1d). Tetrode reconstructions and verification of tetrode tract localization were made based on registration of histological sections to the Waxholm Space Atlas of the Sprague Dawley at Brain v3 (Bjerke et al., 2018; Papp et al., 2014). Coordinates of the craniotomies relative to bregma were: V1 at -6.0 mm posterior, -3.2 mm lateral; S1BF at -3.1 mm posterior, -5.1 mm lateral; PER at -5 mm posterior, -5 mm lateral; CA1, -3.5 mm posterior, -2.4 mm lateral. Within each area a separate reference electrode was inserted. Neural activity was recorded with a 128-channel Digital Neuralynx Cheetah Setup (Neuralynx, Bozeman MT). Spiking activity was extracted from bandpass filtered (600 – 6000 Hz) signals, which digitized one millisecond epochs at 3 kHz when a pre-set voltage threshold was crossed.

Single units were isolated by semi-automated spike sorting (KlustaKwik, Ken Harris, and MClust 3.5, A.D. Redish). As interneurons can show narrow waveforms (Cardin et al., 2009; Gentet et al., 2010, 2012), we could classify neurons as Fast Spiking (FS) interneurons or pyramidal cells (see Vinck et al., 2016 for more details). For spatial linearization of the maze, it was segmented into 51 spatial bins (21 per arm, 9 for the middle lane). Rat position was assigned to a bin by assessing the minimal Euclidean distance between the rat's position and the bin centre position (for additional details see Vinck et al., 2016).

Analyses

Single Neuron – Population Coupling (SNPC). The goal of this analysis was to determine the temporal profile of population activity relative to the spikes fired by a single reference cell. Single-unit activity was collected in 1 ms bins. For each reference cell, the SNPC was calculated relative to a target population, which could be recorded from the same brain area or a different one. When calculating within-area (i.e., internal or local) coupling, the reference cell was not included in the target population. Let the reference cell's firing rate be a $1 \times t$ vector R, with t being the duration of the recording period in ms. The target population firing rate was defined as the $N \times t$ matrix PR, where N is the number of neurons in said target population. To compute the SNPC, the population rate PR was summed across all target neurons to yield the $1 \times t$ vector PR_{sum}. The SNPC was calculated as the crosscorrelation of PR_{sum} with R, with a maximum positive and negative lag of 5015 samples (5 seconds and 15 additional samples for edge-effect corrections), divided by the total amount of spikes in R. The end product of the crosscorrelation was convoluted with a Gaussian kernel (with a half-width of 12 ms, size of 15 samples). Edge effects due to the convolution were corrected by removing the outer 15 samples, resulting in a -5 to +5 second SNPC. If a population had less than 3 cells, we discarded it from further analysis.

Shuffling procedures. To determine the statistical significance of peaks in the SNPC crosscorrelogram, we used a shuffling approach. While keeping the original reference firing rate R, each row of the population rate matrix PR (i.e., firing rate of each neuron in the target population) was shuffled based on a circular temporal shift, with a maximal shift of plus or minus 50% of the entire recording length to get $PR_{shuffled}$. The SNPC-shuffled was calculated from $PR_{shuffled}$ and R, as before. The shuffling procedure was repeated 1000 times. The Z-scored SNPC crosscorrelogram was acquired from the mean and standard deviation of all the $SNPC_{shuffled}$ versus the actual SNPC crosscorrelogram. Physiologically meaningful coupling implies a significant deviation of the SNPC from the $SNPC_{shuffled}$. The level of coupling in standard deviations was quantified as the peak value of the SNPC (where a peak is the highest value flanked by lower values, as determined by the MATLAB default peakfinding algorithm). We defined a cell as 'coupled' if the SNPC was 4.5 std or higher above baseline, which also provided the basis for the Broadcasting Index (see also 'statistical analysis', below).

Spatial selectivity. Spatial selectivity was quantified in bits per spike (Skaggs, McNaughton, & Gothard, 1993):

$$I = \int_x \frac{r(x)}{r} log_2 \frac{r(x)}{r} p(x) dx$$

which calculates *I*, the spatial information (in bits per spike), where *x* denotes the current spatial bin, *r(x)* is the mean firing rate at bin *x*, *r* is the overall mean firing rate of the neuron, and *p(x)* is the probability density for the rat's position. Clustering of CA1 spatial selectivity and coupling values was performed with a K-means clustering algorithm. Clustering was performed on log-transformed data, with the aim to find two clusters. For Fuzzy clustering, a Fuzzy C-means clustering algorithm (Fuzzy Clustering and Data Analysis toolbox, abonyilab.com/fclusttoolbox) was used. Here, cluster identity was defined by having a fuzzy partition above 0.75.

Non-REM sleep, quiet wakefulness and awake wakefulness. We compared three brain states: an awake but largely inactive state during the inter-trial interval (ITI), task performance (TP) and non-REM sleep (NREM). ITI was identified as the period between the animal's return to the central arm (i.e., the start of the intertrial interval, ITI) and sound cue indicating onset of a new trial. This period lasted 19.0 ± 0.05 s (mean ± SEM) per trial. The TP period was taken from the active part of the trial and ranged from visual stimulus onset to the return to the central arm. This period lasted 23.5 ± 0.42 s (mean ± SEM) per trial. After the period of task performance, the animal was allowed to sleep in a towel-covered flowerpot during which recordings continued. NREM sleep periods were identified by visual inspection of video footage and LFP traces as characterize by an absence of body movement and prominence of sharp wave-ripples and large-irregular activity (LIA) in the hippocampal leads (cf. Lansink et al. 2009). Bouts of NREM sleep lasted 47.7 ± 1.33 s (mean ± SEM).

Correlation coefficients between total coupling profiles of the different brain states were calculated for individual sessions. Individual sessions provided three coupling profiles (i.e. 4x4 matrices) for the three brain states, defined as the median coupling for each combination of available areas in said session. 2D correlations coefficients were calculated using MATLAB's *corr2*, for each session, between the three different brain states.

Statistical analysis. Under all conditions, and for all areas, levels of SNPC were not normally distributed, as shown by a Kolmogorov-Smirnov goodness of fit test. Hence, non-parametric testing was applied wherever possible. The Kruskal-Wallis test was used to determine an effect of each combination of reference and target area. The Wilcoxon's rank-sum test was used for pairwise comparison between different population coupling levels. Notably, the within-area and between-area groups were handled separately because the marginally large SNPC values of the within-area group would skew any statistical analysis severely (note that the within-area group consisted of the four available areas coupled with themselves; between-area groups consisting of the four available areas coupled with the three other areas, resulting in a total of twelve combinations)). All correlations (within-area versus between-area coupling, spatial-selectivity versus coupling) were quantified using Spearman's rank correlation. To identify significant effects of correlations, a Kruskal-Wallis test was performed on data

binned along the explanatory variable (i.e., within-area in figure 4, spatial selectivity in figure 6). Bins were determined with the Freedman-Diaconis' method. The same statistical assumptions hold for the correlations between coupling levels and spatial selectivity. Lastly, if both brain area and brain state served as independent variables, we used a Schreier-Ray-Hare test, followed up by Wilcoxon's signed-rank (in paired conditions) or Wilcoxon's rank sum (in unpaired conditions) test for differences between states within one set of brain areas. All P-values were Bonferroni-corrected for the number of comparisons. Lastly, we define the Broadcasting Index (BI) as the number of areas a single cell is significantly coupled with (excluding the area containing that cell). We qualified peaks of the Z-scored SNPC above 4.5 standard deviations (or $p = 6.8 \times 10^{-6}$) to be significantly coupled. To estimate how likely connections to two or three areas are, we compared bootstrapped (N=1000) significant connections (i.e. SNPC above 4.5 standard deviations) to either two or three target areas with the joint probability calculated from probabilities of having any connecting to the respective target area. Here, we defined significance as having a joint probability outside of the 5 to 95% confidence intervals from the bootstrapped data (fig. 5a). To compare percentages of cells with different broadcasting indices per area, a bootstrapping procedure (1000 repetitions) was applied. Proportions of cells with a particular BI with nonoverlapping 5 and 95% confidence intervals were deemed significantly different (fig. 5b).

2.4 Results

Within-area coupling

We performed tetrode recordings while rats (N = 3) navigated a figure 8-maze (fig. 1A, B). We isolated single unit activity (total 1781 neurons) from S1BF, V1, PER and CA1 (fig. 1C, D) For the SNPC, we calculated Z-scored, within-area coupling, cross-correlating single unit activity with summed population activity (fig. 2A). SNPC was calculated for all four areas, first assessed during active wakefulness. Our hypothesis held that within-area coupling would be homogeneous across the neocortical areas with likely stronger within-area coupling in the hippocampus, based on its strong propensity to generate synchronous rhythmic activity (Buzsáki, 2010). Regardless of the brain area, over 80% of all cells showed a peak centred at zero lag (fig. 2, table S1), indicating that these cells were spiking often near-synchronously with numerous other units from the same population. In all areas, a number of cells showed a lack of a strong central peak, as expected from earlier studies in V1 (e.g. fig. 2B; green line; cf. Okun et al., 2015). A Kruskal-Wallis test indicated a strong difference between average levels of population coupling of the four areas (performed on only within-area data, Chi-square = 408.28, $P < 10^{-5}$, df = 3). Notably, we observed a high level of within-area coupling in the hippocampus compared to perirhinal and sensory cortices (fig. 2C; CA1 vs S1BF, V1 and PER: all $P < 10^{-5}$, Wilcoxon's rank-sum test). In the somatosensory and visual cortex we observed similar levels of coupling. Lastly, perirhinal cortex showed significantly weaker within-area coupling compared to S1BF and area CA1 (both $P < 10^{-5}$), but not visual cortex. In sum, these within-area coupling results are in line with earlier studies on population coupling in V1 and show a relatively large heterogeneity across the four areas, with area CA1 showing markedly high levels of within-area coupling.

Between-area coupling: general observations

Between-area coupling was studied by correlating activity of a single unit from one area with the population activity of another (fig. 3A). We hypothesized that the coupling between two distinct sets of areas will basically conform to anatomical patterns of connectivity. Every single combination of areas contained units displaying a noticeable peak around t = 0 (fig. 3, table S1), signifying a cell being coupled between the two areas in question. Generally, between-area SNPC profiles were more temporally spread out and more variable compared to within-area SNPC. Fewer neurons showed very high coupling, and on average, coupling values were lower than for within-area SNPC patterns (fig. 3C, C, S1). As all coupling values are Z-scored values against a shuffled distribution, these data indicate that a neuron coupling to an external area is, on average, less tightly correlated in comparison to local coupling. A Kruskal-Wallis test indicated a strong difference in coupling levels for all between-area combinations (performed on only between-area data; Chi-Square = 221.88, $p < 10^{-5}$, df = 11). For the sake of clarity, we will next discuss these between-area results in three categories: sensory cortices (S1BF and V1), perirhinal cortex and hippocampus. The two sensory areas are deemed to have relatively similar neocortical circuitry, considerably different from perirhinal and hippocampus, as such they are grouped together (Douglas & Martin, 2010; Harris & Shepherd, 2015).

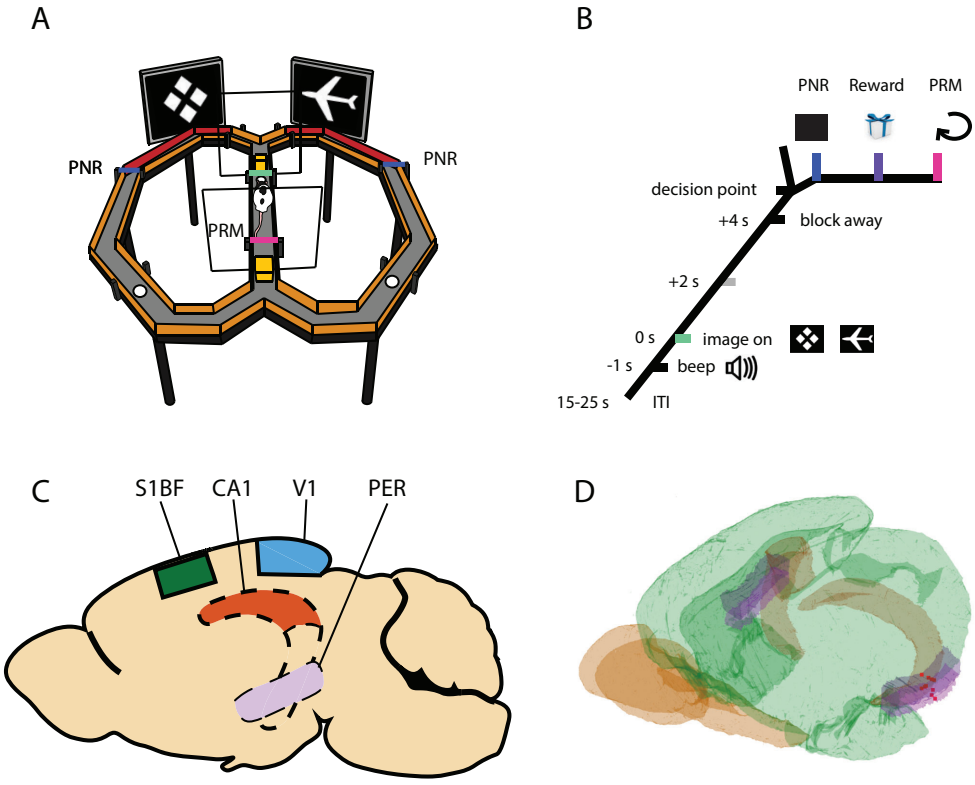

Figure 1: Animals performed a behavioural task on a figure-8 maze, during which recordings were performed from S1BF, V1, PER and CA1. (A) A schematic depiction of the figure-8 maze. Images were presented on monitors along the initial segments of the alleys. Crimson edges below the visual stimulus indicate sandpaper-walls. White dots represent reward wells. Green, blue and magenta lines represent closable barriers in the animal's behavioural progression of the trial; a frontal barrier in the middle lane (green; trial start point), Point of No Return (PNR, blue) after which the animal cannot return to correct its decision, and the Point of No Return Middle (PRM, magenta), the posterior barrier of the middle lane. (B) The temporal structure of the behavioural task. 'Block away' marks the time point at which the green barrier was removed to enable the animal to execute its choice. ITI: intertrial interval. (C) Sagittal view of the recorded areas: S1BF (green), V1 (blue), PER (violet) and dorsal CA1 region of the hippocampus (orange). (D) Example 3D reconstruction of tetrode recording locations in PER of one animal. The red dots represent the reconstruction of the endpoints of respective tetrodes targeting the PER.

Coupling of sensory cortical neurons with populations in other areas
We expected to see coupling between sensory areas, and from sensory areas to perirhinal, as these have shown to be directly anatomically connected (Agster & Burwell, 2009; Burwell & Amaral, 1998, Iurilli et al., 2012; Meijer et al., 2017; Naber et al., 1999, 2000; Zakiewicz et al., 2014). Sensory areas were not expected to couple strongly with the hippocampus due to the indirect connectivity. Taking S1BF neurons in relation to V1

populations ($S1BF_{cell}$ – $V1_{pop}$), and vice versa ($V1_{cell}$ – $S1BF_{pop}$) we found a mean Z-scored coupling level of 4.83 and 6.42 std, with a median of 3.91 and 5.13 std respectively, and noticeable spread to higher values, with outliers above 20 std (fig. S1). These outliers represent single neurons with very strong spike synchronization relative to the other sensory cortical area. Interestingly, V1 units were more strongly coupled to the S1BF population than the other way around (fig. 3C, S1, $P < 10^{-5}$, see also table 2). Next, our data showed low coupling of sensory areas with perirhinal cortex compared to coupling of the two sensory areas to each other. Lastly and surprisingly, S1BF cells showed significantly elevated coupling with CA1 populations compared to other target areas ($P < 0.0005$), while V1 cells lacked strong coupling with the CA1 population (however, this connection showed strong outliers). The coupling of both sensory areas to CA1 showed noticeable outliers. $V1_{cell}$-$CA1_{pop}$ and $S1BF_{cell}$-$CA1_{pop}$ coupling did not differ significantly. For an overview of testing for statistical significance, see table S2. These results indicate that spike-based coupling between sensory areas and parahippocampal areas diverges from predictions based on anatomy.

Coupling of perirhinal neurons with populations in other areas

As an area intermediate between sensory areas and hippocampus, perirhinal cortex was expected to be coupled with both sensory areas and hippocampus. Moreover, perirhinal neurons locking to CA1 theta oscillations (Bos et al. 2017) may be expected to show strong coupling. However, of all four areas studied, perirhinal neurons showed the lowest level of between-area coupling, with less outliers (fig. 3, S1). PER cells engaged in significant SNPC with the sensory cortices, albeit less than SNPC levels between these two sensory areas. PER neurons coupled noticeably less with V1; in this respect their coupling was similar to that of V1 neurons, showing low coupling with PER. Furthermore, PER neurons showed stronger coupling to hippocampal populations (PER_{cell} – $CA1_{pop}$) and S1BF (PER_{cell} – $S1BF_{pop}$) than to V1 populations, which was of comparable level as the sensory neurons with CA1 populations (i.e., not significantly different, see table S1). Interestingly, the overall coupling profile does not appear to differ much from the other two neocortical areas (see also table S2). These results highlight PER as an overall weakly coupled area, but its strong coupling with CA1 populations agrees with earlier studies.

Coupling of hippocampal neurons with populations in other areas

Our data showed a modest level of functional coupling for $CA1_{cell}$ – PER_{pop} (fig. 3, S1), of comparable value as PER_{cell} – $CA1_{pop}$, and with relatively low outliers (e.g. below 20 std, fig S1). Area CA1 cells showed similar levels of coupling with sensory cortices, noticeably with strong outliers, especially with the V1 population. Interestingly, CA1 cell couplings to all three target areas were not significantly different from each other (fig. S1, table S2). Thus, unlike the anatomic connectivity would suggest, CA1 cells are equally coupled to the sensory cortical areas and to PER populations, with some outliers to sensory areas.

Cell types

Fast spiking (FS) interneurons and pyramidal neurons were classified by way of waveform shape and firing characteristics (putative interneurons, N = 188; putative pyramidal neurons, N = 1593). We hypothesized FS interneurons and pyramidal neurons to

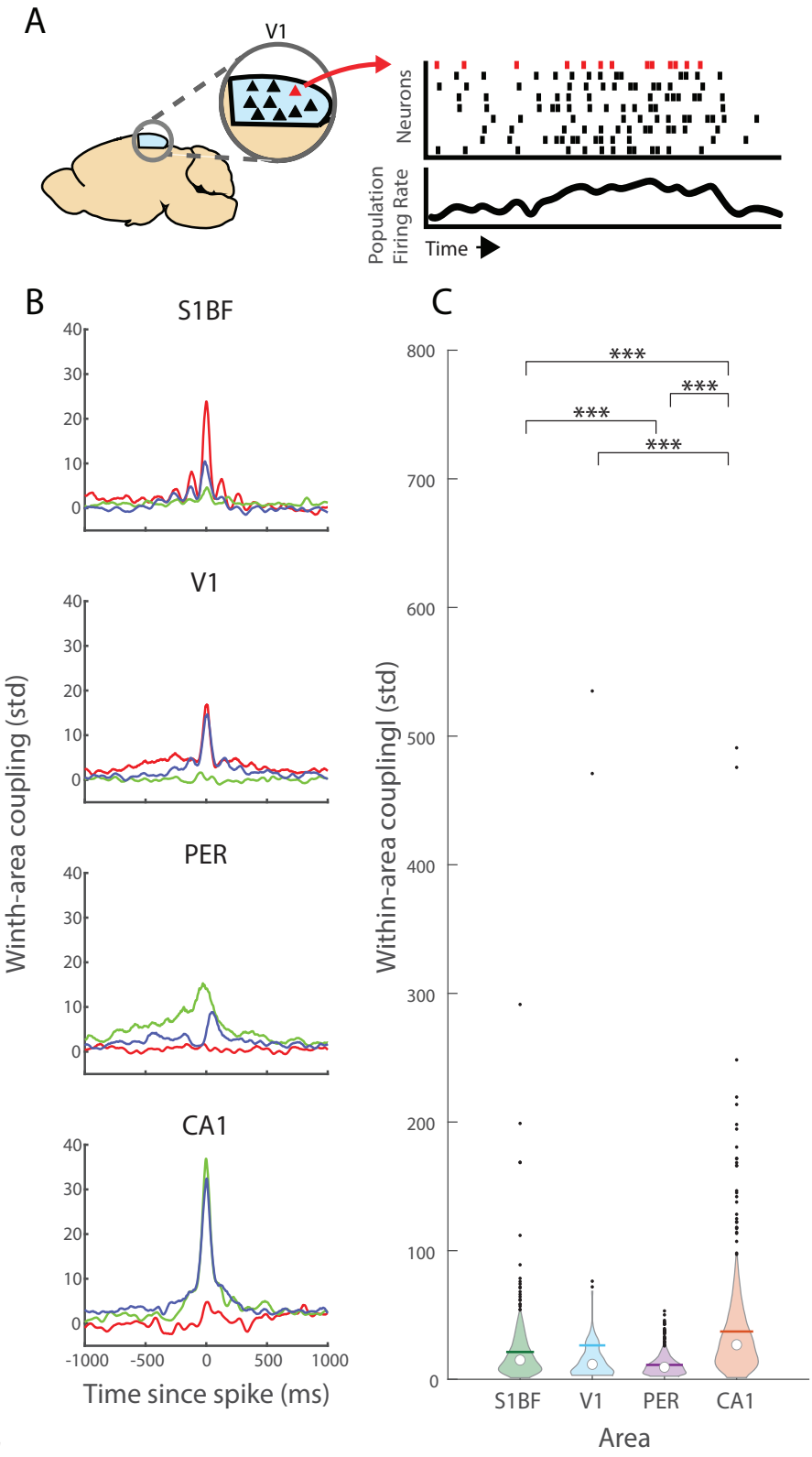
A
V1
Neurons
Population Firing Rate
Time
B
S1BF
V1
PER
CA1
Winth-area coupling (std)
Time since spike (ms)
C
Within-area couplingl (std)
***
***
***
***
S1BF
V1
PER
CA1
Area

◀*Figure 2: Within-area single-neuron population coupling shows divergence between strongly and weakly coupled cells. (A) The within area SNPC was calculated from spiking activity within a single area (left, only V1 is depicted). V1 spiking activity is summated and cross-correlated with single unit activity (right), for example: comparing the red spikes with the total population activity (bottom right). (B) Representative SNPC within single areas, Z-scored to shuffled distribution, of four reference cells being coupled with the population within the same area, for each of the four recorded areas. Note the diversity in peak height, and the lack of a peak for some units, such as the green cell in V1. Each differently coloured line indicates a different reference cell. Barrel cortex displays oscillatory activity in the low theta range (~7 Hz) as noticeable oscillations in these graphs. (C) Violin plots showing spread and average of the within-area population coupling of all units of all animals. White dot: median; horizontal line: mean; black dots are > 95% percentile outliers. The areas are represented as green (S1BF), blue (V1), violet (PER), orange (CA1). *** indicates p < 0.0005. P-values are Bonferroni corrected for 6 tests.*

show markedly different coupling profiles, with FS interneurons being strongly locally interconnected, whereas pyramidal neurons were expected to be more strongly coupled to more distant populations. However, when putative pyramidal and FS interneurons were analysed separately, within-area coupling showed a similar pattern as when all neurons were combined, accompanied by roughly similar significant differences (albeit different P-values, fig. S2). An exception was found for the two sensory areas: FS interneurons in S1BF showed higher within-area coupling than V1 FS interneurons, which was not the case for pyramidal cells. FS interneurons showed an overall higher level of within-area coupling than pyramidal cells, yet this was only significant for area CA1 (Wilcoxon rank-sum, pyramidal neurons vs. FS interneurons for CA1, $P < 10^{-5}$) and to a lesser extent S1BF ($P < 0.05$; see table 3 for statistical testing of differences between within-area coupling for pyramidal and FS interneurons).

As concerns between-area coupling, putative FS interneurons and pyramidal cells showed a surprisingly similar pattern (fig. S3). Overall, FS interneurons tended to show higher levels of coupling to other areas than pyramidal cells, although this was only significantly different for three areas (table S4), most noticeably for $CA1_{cell}$ - $S1BF_{pop}$. Thus, the overall pattern we observed when all cells were combined, as described above, was largely preserved for the two different neuron types (see table 4 for statistical testing of differences of all between-area coupling combinations for the two different cell types; see table 5 for statistical testing of between-area coupling of pyramidal cells versus FS interneurons).

Intra-areal coupling selectively correlates with inter-areal coupling

Could there be a relation between a cell's local and global coupling patterns? If single cells can play a pivotal role in regulating meta-network activity, one might expect a cell's within-area coupling to be predictive of between-area coupling: a strong locally connected cell may be in an ideal situation to convey information to an external target. Figure 4 displays the relations between within-area and between-area coupling for four reference areas with selected target areas with linear regressions displayed for significant correlations (see fig. S4 for individual plots for all reference-target combinations).

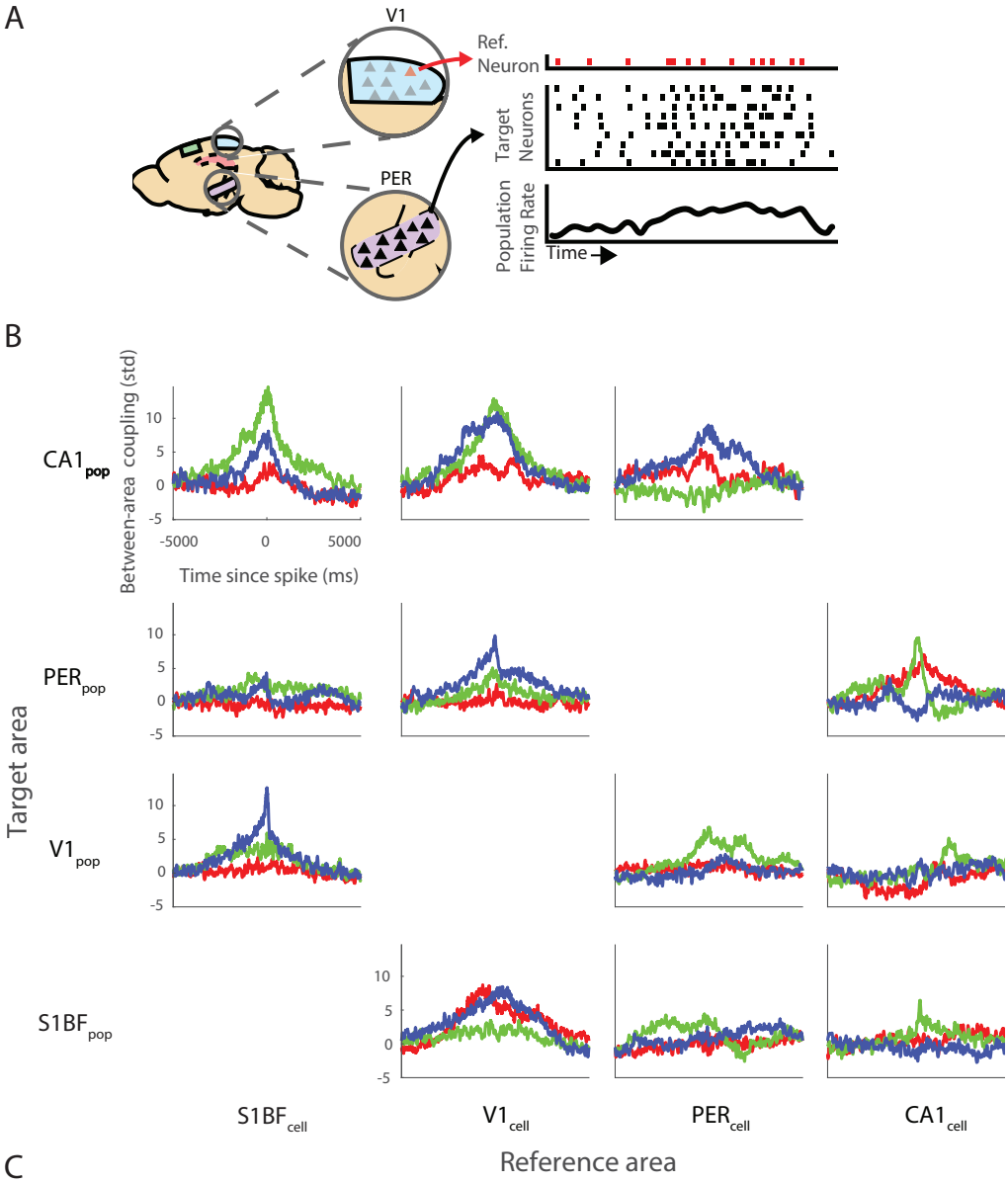
A
V1
Ref.
Neuron
Target
Neurons
PER
Population
Firing Rate
Time
B
CA1pop
Between-area coupling (std)
10
5
0
-5
-5000
0
5000
Time since spike (ms)
PERpop
V1pop
S1BFpop
Target area
S1BFcell
V1cell
PERcell
CA1cell
Reference area
C
CA1
PER
V1
S1BF
3.5 std
5.1 std

◀*Figure 3: Between-area single-neuron population coupling shows how single neuron activity related across great anatomical distance to other populations. (A) schematic illustration of between-area coupling, comparable with figure 2A. The spike train of a single unit in a given area (e.g., V1, left) is correlated with the population activity of another area (e.g., PER). The red example neuron is cross-correlated with the total population rate of the target area (right). (B) Representative SNPC between areas, Z-scored to shuffled distribution, between different areas, excluding within-area coupling at the diagonal. Note a longer time range on the X-axis than used in figure 2b. Columns correspond to reference areas, i.e., the areas to which the single neurons belong, rows correspond to the target areas, i.e., the areas to which the population rate signals belong. Differently coloured lines per individual plot denote different cells from the reference area. Note the lower central peaks, and the broader temporal spread, compared to figure 2b. As opposed to the within-area cases, most cells do not show strong coupling, however several units are strongly coupled, e.g. the green line indicating an S1BF cell with the CA1 population. (C) Schematic depiction of median coupling levels across sessions, expressed as Z-scored SNPC, between the different cells and areas. Line thickness scales linearly with median coupling strength. Across all images the areas are represented as green (S1BF), blue (V1), violet (PER), orange (CA1). Triangles represent single units, the coloured circles the entire population, i.e., a line from one triangle in V1 to the S1BF population depicts the median strength of V1 cells to the S1BF population.*

Data showed mostly moderate to weak correlations between within-area coupling and between-area coupling. Interestingly, S1BF showed a significant correlation between its within-area coupling and its coupling to CA1. A similar trend was seen for visual cortex (i.e., V1 within-area versus $V1_{cell}$ – $CA1_{pop}$, where the linear regression was relatively flat despite an increased spread with rising within-area coupling values (fig. S4, second column, top row). Both sensory areas lacked a significant correlation between their within-area coupling and their coupling to the PER population. PER cells showed overall low Spearman's rho values between their within-area coupling and all target areas, indicative of a general lack of within-area SNPC correlation to connected areas. Lastly, within-area coupling of CA1 cells was significantly correlated with coupling to S1BF and PER populations, but not with V1. Overall, we find several connections showing positive correlations between external and internal coupling, however, this was not invariantly shown in all area-to-area combinations.

Broadcasting index

To quantify in more detail how cellular coupling to populations diverges - or broadcasts - across multiple areas, we defined a broadcasting index (BI). The BI is the number of target areas to which the cell under scrutiny significantly couples (4.5 std above shuffled distribution; see Methods). By definition, for each cell this value ranges from zero (no significant coupling) to 3 (significantly coupled to all three target areas). Within-area coupling is not included in the BI. We hypothesized that high-broadcasting cells (BI of two or three) are found in every area, with a higher number in CA1 and perirhinal cortex, because these areas are thought to be hierarchically well-positioned to broadcast to many neocortical areas (Fiorilli et al., 2021; Squire et al., 1989). Much like the within-area versus between-area correlations described above, we would expect high-broadcasting cells to be strongly connected with their local population.

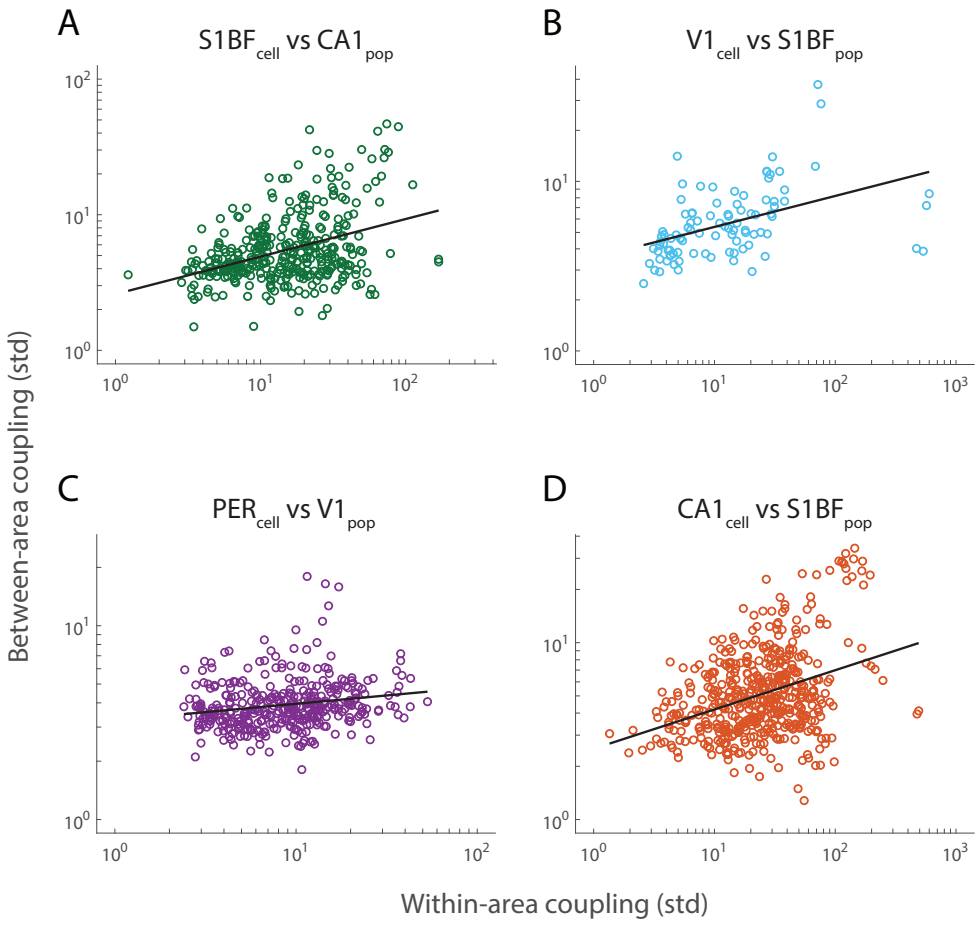

Figure 4: Positive correlations between within-area and between-area coupling. Scatterplots of within-area coupling versus between-area coupling strength for the four reference areas with one selected target area (A to D). X-axis indicates the within-area coupling strength of the reference area, Y-axis indicates the coupling of said reference area with the target area (indicated in the title as 'Ref$_{cell}$ vs Target$_{pop}$'). Each dot represents one cell. Target areas were selected based on the significance of their correlations (a complete overview of all the areas is given in supplementary figure S4). Black lines are linear regressions on log-transformed data. Correlations are quantified as Spearman's rho (from A to D: $\rho = 0.28$, $p < 10^{-5}$; $\rho = 0.57$, $p < 10^{-5}$; $\rho = 0.23$, $p = 0.00015$; $\rho = 0.28$, $p < 10^{-5}$). P-values were Bonferroni corrected for 12 tests. Across all images the reference areas are represented as green (S1BF), blue (V1), violet (PER), orange (CA1).

In every reference area, we found cells that broadcast to all three other areas (i.e., BI = 3), albeit that these constituted only a small minority of the total number of neurons (fig. 5A). In all areas, we found that the amount of cells with a BI of 3 exceeded what would be expected from the joint probability of the single connections, while a BI of 2 often appeared in lower numbers than expected (fig. 5A). Furthermore, we observed a trend with V1 showing more broadcasting cells, yet an effect of area on the amount of cells

with a specific BI was not significant. Comparing percentages of cells with a certain BI across all areas, we saw a general reduction of the ratio of cells with higher broadcasting indices, yet between broadcasting indices 1 and 2 this diverged for the different areas: CA1 and V1 showed no significant difference between indices 1 and 2, while S1BF and PER showed a significant reduction in the number of cells with index 2 compared to 1 (based on bootstrap-estimated confidence intervals, see Methods). No significant differences between the four areas were observed for maximum broadcasting (BI of 3). Lastly, we expected a higher BI to be related to stronger local coupling. Interestingly, however, cells with different broadcasting indices showed no significantly different levels of within-area coupling, for all areas (fig. S5).

Between pyramidal cells and FS interneurons (fig. S6A, B) we observed the same overall decrease in the amount of cells with higher broadcasting indices. FS interneurons showed a significant higher percentage of cells with non-zero broadcasting indices in S1BF and CA1 ($P < 0.05$, bootstrap test), and showed an overall larger variation for each area. (note that the total number of FS interneurons was roughly 7 times less than the number of pyramidal neurons, influencing statistical power and variability). FS

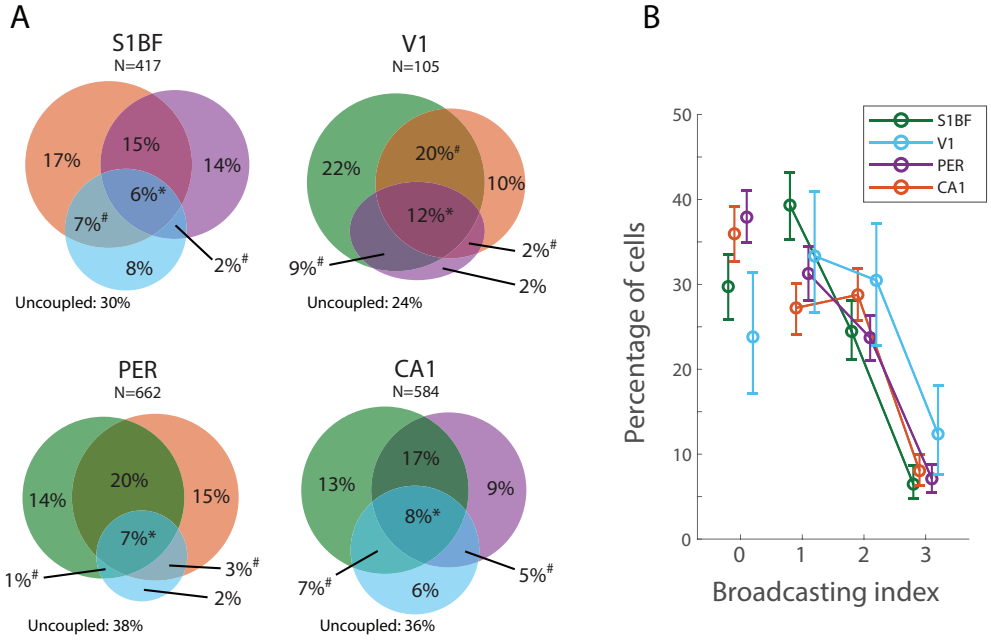

Figure 5: Cells in sensory and (para)hippocampal areas mostly show varying degrees of broadcasting. (A) Venn diagrams illustrating the percentages of cells having a significant amount of coupling to the three available target areas. Asterisks and pound symbols show results for bootstrap testing ($\alpha = 0.05$) if connections to two or more areas are expected compared to the joint probability of cells connecting to one area. Asterisks indicate more cells than expected, and pound symbol less than expected. (B) Percentages of cells plotted as a function of broadcasting index. Confidence intervals are bootstrap estimates (1000 iterations). Across all images the areas are represented as green (S1BF), blue (V1), violet (PER), orange (CA1).

interneurons in PER lacked coupling with V1, resulting in a lack of cells with a BI of 3. Similarly, pyramidal neurons as well as FS interneurons showed no effect of BI on within-area coupling (fig. S6C).

Summarizing, broadcasting cells are found in all areas, and we did not find strong differences between the examined brain areas. Broadcasting appears to be independent of the cell's coupling with its local population.

Population-coupled neurons and spatial selectivity

Within-area population coupling may reflect intrinsic neuronal parameters, largely invariant to cognitive computations. The contrasting hypothesis holds that SNPC does cohere with representational content coded in the area under scrutiny, such as spatial information coded in area CA1 (O'Keefe & Dostrovsky, 1971). Regarding between-area coupling, we hypothesized that spatial selectivity of CA1 cells may be correlated with strong coupling to sensory areas: if the spatial selectivity of CA1 cells is dependent on sensory inputs (Hartley et al., 2000; Jeffery, 2007; Mehta, 2015), coupling of spatially selective cells may be stronger with sensory areas as compared to non-selective cells. Spatial selectivity was calculated in bits per spike (fig. 6A). As expected, we found high levels of spatial selectivity in a subset of CA1 cells during maze running (fig. 6A, B). As reported before, a subset of PER neurons fired selectively for large maze segments (Bos et al., 2017) and a limited location-dependence was observed for both sensory areas (Long & Zhang, 2019), resulting in a low number of cells with high spatial selectivity (fig. 6B). It should be noted that the apparent spatial selectivity of some S1 and V1 cells may be explained by location-specific behaviours which impose local, sensory-specific changes.

We found that, if correlations between spatial selectivity and population coupling were significantly different from zero, they were negative (fig. 6C). As the SNPC is corrected for number of spikes and spatial selectivity is expressed in bits/spike, this effect cannot arise from lower numbers of spikes in cells with higher spatial information. Furthermore, CA1 showed two clusters of higher and lower spatial selectivity (defined with K-means clustering, fig. 6C and S7). When comparing SNPC in these separate clusters, we found a strong significant difference in within-area coupling between the low and high spatially selective groups (fig. S7B, Wilcoxon's rank-sum test, $P < 10^{-5}$). Because some datapoints do not appear to clearly fall in a cluster, we applied fuzzy clustering and tested for differences between datapoints with a partition over 0.75 (fig. S6C), which provided a comparable level of significance.

Next, we analysed spatial selectivity versus between-area coupling. We found significant correlations reciprocally between CA1 and PER and CA1cell and S1BFpop, with relatively low correlation coefficients (fig. S8). Here, too, we were able to separate CA1 neuron couplings to different areas based on clear clusters of higher and lower spatial selectivity (fig. S9). Differences in between-area coupling for the high and low spatially selective groups were only significant for the coupling of CA1 cells with PER populations (fig. S9C, Wilcoxon's rank-sum test, $P < 10^{-5}$).

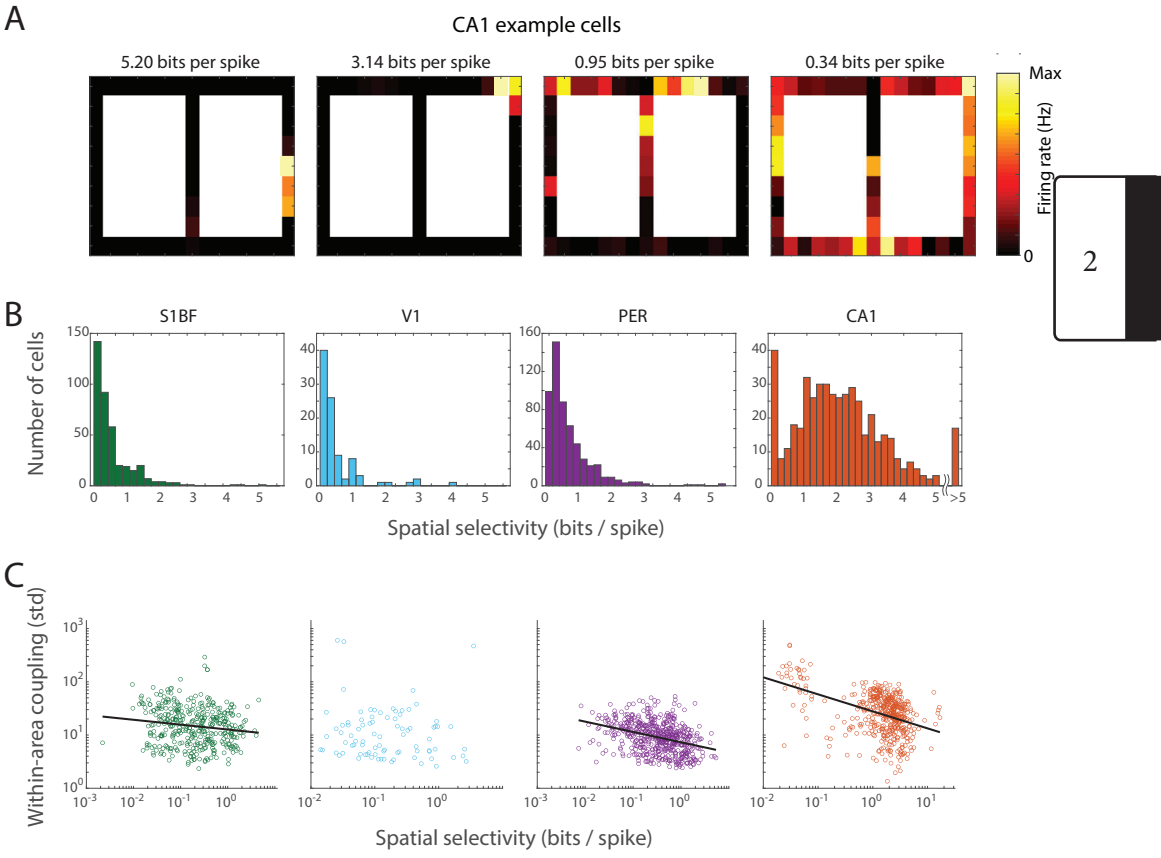

Figure 6: Different areas display differing levels of spatial selectivity, correlated with within-area coupling in S1BF and CA1. (A) Examples of four CA1 cells' spatial responses on the figure eight maze and their respective spatial information in bits per spike. (B) Distribution of spatial selectivity in all four areas. (C) Spatial selectivity correlated with within-area coupling. Black lines are linear regressions on log-transformed data, only shown for significant correlations (from left to right: ρ = -0.16, p = 0.0076; ρ = -0.11, p = 1.2; ρ = -0.38, $p < 10^{-5}$; ρ = -0.38, $p = < 10^{-5}$) . Note that the CA1 population appears to consist of two clusters of cells, based on their spatial selectivity. Across all images the areas are represented as green (S1BF), blue (V1), violet (PER), orange (CA1). All correlations are quantified as Spearman's rho. P values in C are Bonferroni corrected for 4 tests.

Dependence of coupling on brain state

To gain further insight into the dependence of SNPC on intrinsic state parameters vis à vis behavioural conditions, we asked whether coupling, analysed so far in active wakefulness, is affected by brain state. We hypothesized that overall between-area coupling will decrease during non-REM sleep, corresponding to decreased inter-areal communication as compared to active task performance. In addition, we hypothesized that within-area coupling during sleep will increase relative to awake conditions. Lastly, we expected lower levels of between-area coupling in behaviourally active states (Olcese et al., 2016). We classified non-REM sleeping periods (NREM),

inter-trial interval periods (ITI) and active task performance (TP). As expected, these different brain states show different spiking activity, with NREM showing significantly decreased firing rates relative to ITI and TP (fig. S10). First, we assessed brain state-driven differences between overall coupling profiles, i.e. the total profile of coupling of all areas with each other, as a 4x4 matrix. By calculating correlations between coupling profiles during the different brain states we observed that the total profile of coupling per session was different in NREM conditions versus ITI and TP (fig. 7). ITI and TP were highly correlated, indicating no dramatic changes of the total coupling profile between these awake states. The lowest correlations were seen between NREM and TP, however, with a median still above 0.6, indicating that even amongst strongly different brain states, global coupling patterns remain comparable.

The levels of within-area population coupling were selectively affected by state, area and their interaction (fig. 8A, Kruskal-Wallis, $P < 0.05$ for all four areas separately), but remained globally intact across all three states. Post-hoc Wilcoxon's sign-rank tests indicated several significant differences per area. For the sensory areas, coupling in NREM was slightly but significantly elevated in S1BF. Furthermore, V1 displayed a significantly reduced level of coupling in TP versus ITI, a result not shared with S1BF. Next, PER showed significantly higher coupling during NREM versus the other two states. CA1 showed differences between all three states: the highest coupling was found in ITI, followed by TP and lastly NREM. Thus, for S1BF and PER our hypothesis on increased within-area coupling could be confirmed, while CA1 did not appear to follow this pattern, displaying significantly lower coupling in NREM. Furthermore, for V1 we confirmed lower coupling only during TP.

For between-area coupling, we observed no unitary effect of state in all areas, such as a global loss during NREM sleep in between-area coupling (fig. 8B, S11). Overall, we found an effect of state only for CA1 cells and for PER_{cell} - $S1BF_{pop}$ (Kruskal-Wallis, $P < 0.05$). Using a post-hoc Wilcoxon's sign-rank test, these effects were visible as a decrease of coupling of CA1 to all three target areas during NREM, which was significantly lower

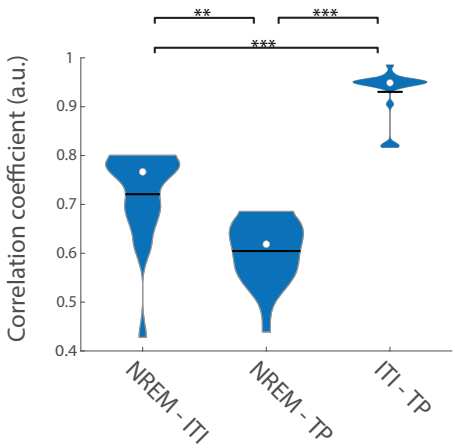

*Figure 7: Correlations of all coupling levels between different brain states, for each session. For each session, correlation coefficients of entire coupling profiles (i.e., all four areas with each other) for two brain states were calculated. The awake states (ITI and TP) are very strongly correlated, while NREM is significantly correlated (although less) with both awake states. White dot: median; horizontal line: mean. NREM: non-REM sleep, TP: task performing, ITI: inter-trial interval. Significance was assessed with Wilcoxon's rank-sum test, ** $P < 0.005$, *** $P < 0.0005$. P-values are Bonferroni corrected for 3 tests.*

than ITI and TP states. Furthermore, PER_{cell} - $S1BF_{pop}$ showed an increase in coupling in NREM sleep relative to ITI. Thus, these results confirm our hypothesis on loss of inter-areal connectivity in NREM sleep only for CA1.

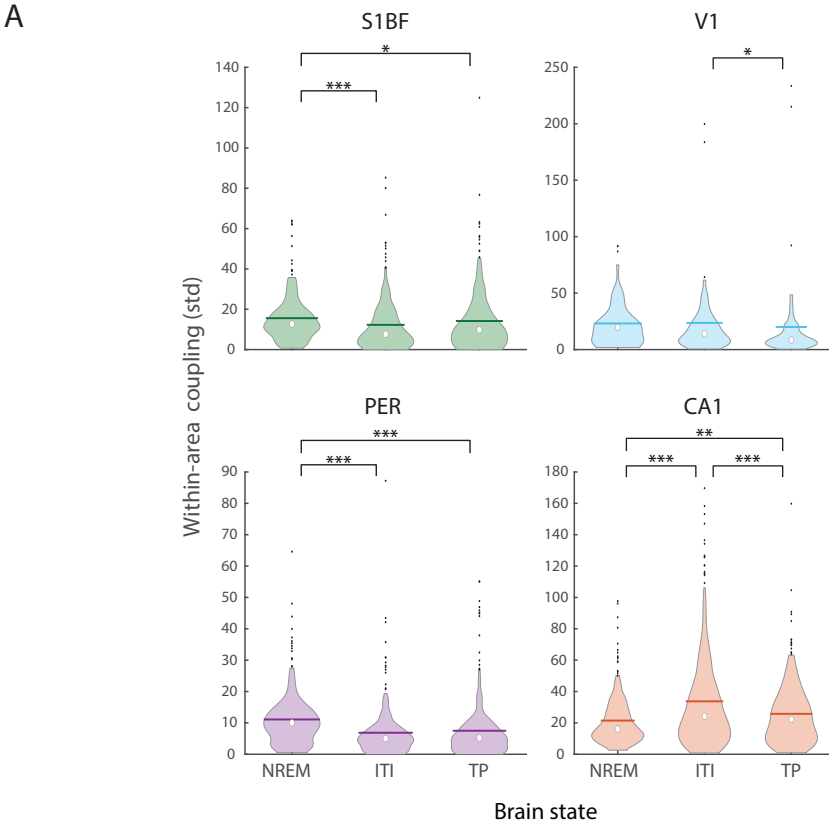

◀*Figure 8: Modulation of within-area and between-area coupling by brain state. (A) Violin plots of within-area coupling in the four areas in the three brain states. White dot: median; horizontal line: mean; black dots are >95% percentile outliers. (B) Median of between-area coupling as a function of brain state. Error bars indicate 5-95% confidence intervals. Significance bars with symbols (e.g., the triangle) indicate which individual coupling value shows significant differences between brain states. Horizontal black bars in the rightmost plot indicate significance between brain states for all three target areas in question. Across all graphs, the areas are represented as green (S1BF), blue (V1), violet (PER), orange (CA1). NREM: non-REM sleep, TP: task performing, ITI: inter-trial interval. The significance of differences between coupling values in different brain states was assessed with Wilcoxon's sign-rank test, * $P < 0.05$, ** $P < 0.005$, *** $P < 0.0005$, horizontal black bar in B indicate $P < 0.05$ for all three target areas in question. P-values are Bonferroni corrected for the number of tests (12 in A, 48 in B).*

2.5 Discussion

We investigated how single-neuron spike patterns correlate with population firing activity within and between sensory cortical and (para)hippocampal areas, with special emphasis on cross-areal interactions. Our main findings can be summarized as follows: (i) coupling of single neurons to their local population was prominent across all four areas investigated, and area CA1 showed a markedly stronger within-area coupling than the other areas (fig. 2); (ii) between-area coupling showed broader and more variable temporal profiles than within-area coupling (fig. 3); (iii) a majority of relationships between within-area and between-area coupling showed significant positive correlations, especially when involving area CA1 (fig. 4); (iv) broadcasting cells were found in all four areas, where higher broadcasting appeared uncorrelated with local coupling (fig. 5); (v) negative correlations were found between spatial selectivity and within-area coupling in S1BF and CA1 (fig. 6), and (vi) although within-area coupling patterns were subject to modulation by brain state, we found between-area coupling values to be generally preserved, except for CA1 in non-REM sleep (fig. 8b). These results characterize the S1BF-V1-PER-CA1 system as a coherent, dynamic meta-network with differentiated degrees of internal and external coupling. In this multi-area system, coupling strengths appear not to be governed primarily by selective information processing expressed during behaviour (e.g. spatial selectivity), but cohere more strongly with intrinsic dynamic properties subject to modulation by brain state.

Within-area coupling: contrast between hippocampus and perirhinal cortex
Our results on within-area coupling in rat cortex are largely in line with previous reports on mouse V1 (Okun et al., 2015) and prefrontal cortex (Okun et al., 2019). The two sensory cortical areas we investigated, S1BF and V1, showed comparable levels of within-area coupling, which is consistent with the general similarity in sensory neocortical wiring conforming to principles of canonical cortical microcircuits (Douglas & Martin, 2004). CA1 harbours densely packed, synchronized populations, acting as a powerful dipole layer that generates high-amplitude LFPs to which neuronal firing is entrained (Buzsaki, 2002; Buzsáki, 2010; Csicsvari et al., 2003; Somogyi, 2010; Yang et al., 2014). This entrainment could be an important factor in accounting for the strong within-area coupling of CA1 neurons. Furthermore, the increased within-area coupling of FS interneurons might link to their prominent role in regulating brain dynamics. Of the four areas studied, perirhinal cortex showed the lowest level of within-area coupling, albeit not significantly lower than V1. Although perirhinal cortex is usually deemed to conform to canonical cortical circuitry, it deviates in some aspects, such as a lower density of pyramidal neurons (Kealy & Commins, 2011). PER has been described as an 'inhibitory wall', gating information flow from the neocortex to hippocampus (de Curtis & Paré, 2004; Martina et al., 2001; Pelletier et al., 2004) and PER has been reported to lack strongly synchronized activity (Pelletier et al., 2004). This might be reflected in the relatively low levels of within-area coupling of PER neurons.

Between-area coupling: deviations from predictions based on neuroanatomy
In general, between-area coupling was less strong and more temporally dispersed than within-area coupling. This difference was expected because connection probabilities

decrease over longer anatomical distances (Ercsey-Ravasz et al., 2013), the involvement of poly- instead of monosynaptic circuitry increases with distance, and a given neuron in a remote target area likely receives inputs from many other afferent areas than from the area containing the reference cell alone.

We found asymmetric coupling levels between the two sensory cortical areas: V1 neurons showed significantly higher levels of coupling with S1BF populations than from S1BF neurons to V1 populations. (Fig. 3, S1, table 2). In line with this, a previous study reported entrainment of V1 neurons by LFPs recorded from somatosensory cortex (Sieben et al., 2013). Theoretically, if firing rates in both sensory areas were the same, it would be mathematically unlikely to have different coupling levels between two reciprocally connections (note that firing rates differ between areas, e.g. fig. S10, yet it is unknown how different firing rates affect coupling specifically). As yet, we can only speculate why the V1-S1 coupling shows an asymmetry. During task performance, intense whisker and other tactile inputs may predominate over visual inputs. $V1_{cell}$-$S1BF_{pop}$ coupling was higher compared to $S1BF_{cell}$-$V1_{pop}$ coupling during NREM sleep (Fig. S11), but this was not significant. As yet, it is too early to ascribe the difference in coupling to sensory inputs arising during active behaviour.

Strikingly, sensory cortical neurons showed higher coupling with CA1 populations than with the anatomically more proximal and more connected perirhinal cortex. Anatomic consensus holds that sensory cortical information is relayed via the perirhinal and postrhinal cortices to the hippocampus (Agster & Burwell, 2009; Arszovszki et al., 2014; Burwell, Rebecca & Amaral, David, 1998; Deacon et al., 1983; Naber et al., 1999, 2000; Witter et al., 2000; Zakiewicz et al., 2014). A strong between-area SNPC may, however, not only reflect sensory input to the hippocampus, but could also express how CA1 population output correlates with single-cell activity in sensory cortices. Such correlation might be driven by brain-wide effectors such as sensorimotor feedback. Likewise, the low coupling between sensory areas and perirhinal cortex diverges from the anatomically based prediction. Again, following the concept of PER as an 'inhibitory wall', a sensory-to-hippocampal gating function may result in a sparsification of PER firing patterns, and hence may result in lower levels of coupling between PER and the sensory cortices. However, if PER would simply function to critically suppress neocortical inputs en route to the hippocampus, one would not expect the strong sensory-CA1 coupling like we observed (fig. 3, S1). This strong coupling may be most parsimoniously explained by sensory cortical-hippocampal connections bypassing the PER (Agster & Burwell, 2009; Fiorilli et al., 2021; Goode et al., 2020; Naber et al., 1999). In general, we note that fiber tracer studies can only provide a crude guidance in predicting SNPC relationships; they establish global innervation patterns but neither probe synaptic connectivity to specific cell types, nor synaptic strength. Thus, tract-tracing and spike-based studies reveal different aspects of interconnected meta-networks and are largely complementary to each other.

Turning to the involvement of putative pyramidal cells and FS interneurons in within- and between-area coupling, we found surprisingly few differences. Although

FS interneurons generally have only local, short-range connections, several studies on hippocampal and rhinal regions showed FS interneurons to project outside their area of origin (Apergis-Schoute et al., 2007; Jinno et al., 2007; Melzer et al., 2012). A possible explanation for the elevated between-area coupling of FS interneurons (fig. S3) may be their role in synchronizing pyramidal neurons, which thereby involve these FS interneurons in between-area interactions via a polysynaptic route. In CA1 and S1BF, interneuronal within-area coupling was, on average, higher than for pyramidal neurons – a result that may likewise be explained by the entraining or synchronizing effect of interneuron activity on mass pyramidal cell activity within the same region (Csicsvari et al., 1999).

Within-area versus between-area coupling and the existence of broadcasting cells

For 9 out of 12 area-to-area combinations, we report significant positive correlations for within-area versus between-area coupling (Fig. 4, S4). This finding supports that a locally coupled cell tends to couple significantly to an external population (Clancy et al., 2019), but it should be noted that most of the correlations had modest Spearman's rho values, implying a great degree of cell-to-cell variability in the relationship between internal and external coupling. Strong local synchrony, corresponding to within-area correlation, would indeed be expected to either correlate with strong afferent input to the same area, or be conducive to driving coordinated output - in both cases leading to a stronger level of between-area coupling (Stevens & Zador, 1998; Zandvakili & Kohn, 2016). Perirhinal cortex was the only target population where coupling with sensory neurons showed no significant correlation between within-area and between-area coupling. For understanding meta-network functioning, this finding indicates that positively correlated within- and between-area coupling cannot be taken to represent a general connectivity rule.

The 'inhibitory wall' property of the perirhinal cortex might act to transform cortical to parahippocampal activity, where neocortical input has a low probability of driving PER neurons to spiking (de Curtis & Paré, 2004; Pelletier et al., 2004). This sparsification would indicate that sensory information gated in perirhinal cortex need not be from 'hub'-like sensory neurons with strong local involvement, but from a broad range of sensory cells. Furthermore, the neocortical-to-parahippocampal transformative properties would predict that CA1 neurons also lack within-vs-between correlation with the sensory areas. However, CA1 neurons coupling with S1BF and V1 showed overall positive correlations. Although this might be explained by differential pathways of information transfer from neocortex to hippocampus (Somogyi, 2010), the exact neuronal variables driving the differences in between-area coupling remain unknown.

The observation of positive correlations between internal and external coupling gave rise to the hypothesis that broadcasting or 'hub' cells may exist – neurons significantly coupled to more than one area. Such cells were identified in all four areas, and especially neurons with an index of three were more often found than expected by chance. The distribution of broadcasting indices did not vary greatly between areas and did not

markedly differ between different cell types (Fig. S6). Widely broadcasting cells might indicate important synchronizing nodes in a small-world-like network (Bassett & Bullmore, 2017; Watts & Strogatz, 1998). Because broadcasters engage in synchronizing relationships with multi-area populations, they may function to integrate information, and dynamically coordinate activity in single-area networks, thus contributing to the formation of meta-networks (Pennartz, 2015) or network-of-networks (NoNs; e.g. (Havlin et al., 2015). Notably, broadcasting cells did not show strong within-area coupling, indicating involvement in the local circuit does not correlate with a cell's broadcasting properties. If, however, broadcasting cells are sufficiently connected to neurons with strong within-area coupling, then such internal coupling can still influence spiking synchronization in multiple connected areas.

Negative correlation between spatial selectivity and single-neuron population coupling

The negative correlation we found between spatial selectivity and local population coupling of CA1 neurons was mirrored by similar findings in S1BF and PER (fig. 6). At first sight this negative relationship may seem surprising, but a strong functional connectivity of a given neuron to its local population may well be accompanied by a plethora of mixed inputs to this neuron, preventing it from generating a highly specific spatial code. Indeed, a recent study found synaptic glutamatergic input to non-place cells to be slightly but significantly higher than place fields (Adoff et al., 2021). Secondly, our findings indicate that high SNPC is not driven by local neurons with high spatial selectivity. Had within-area coupling been driven by the animal's locomotor behaviour leading to sequential activation of place cells in CA1, then a positive correlation would have been expected. Thus, SNPC in areas CA1 and S1BF is not strongly determined by cognitive computations underlying place tuning.

Modulation of population coupling by brain state

We report several differences in single neuron-population coupling between awake (i.e. task-performing and non-performing states) and non-REM sleep. First, the high correlation between the active and passive awake states indicates overt behaviour has little effect on general patterns of coupling between brain areas. Furthermore, although coupling patterns are different between non-REM conditions and awake states, the correlation between these states is far from abolished. Thus, between different brain states, coupling remains largely driven by internal dynamics. During non-REM sleep, we expected a general decrease in between-area coupling, but an increase in within-area coupling (Olcese et al., 2016). Within-area coupling indeed increased during sleep in most areas, with CA1 forming an exception. Furthermore, we did not find a clear decrease of between-area coupling between areas, again with CA1 being the exception: for CA1 all between-area connections were lower than during awake conditions. Although loss of cortical integration has been theorized to be an integral part of the loss of consciousness (Alkire et al., 2008), the current data suggests that on the cell-to-population level, this lack of integration only appears between hippocampus and cortical areas. A cell-to-cell measure, for instance as used Olcese et al. (2016) shows different results, highlighting the different levels of processing at ascending scales of

brain function. As yet, it remains unknown what drives these differences.

In a final assessment of the data, it is appropriate to re-examine what an elevated SNPC reflects, and what its functional significance may be. As SNPC correlated negatively with specific information-coding – illustrated here especially by the spatial selectivity of CA1 cells – it is most parsimoniously interpreted as an expression of intrinsic network dynamics, offering a time-averaged window on cell-to-population synchronization. Our findings show that single neurons not only synchronize with their local network, but also with other populations in the hippocampal-neocortical network, and may thus primarily function in dynamically organizing communication in such large, cross-areal systems. However, when one adopts the reverse perspective and focuses on those cells that do not conform to the population firing regime ('soloists'; Okun et al. 2015), one does identify subgroups of neurons having specific information-processing functions. Desynchronized from internal and/or external networks as these cells are, they may guarantee a required level of sparse neural coding (Goltstein et al., 2015) and prevent the overall network from reaching a state of hyperstability during wakefulness. They form an intriguing target of future investigation of ensemble behaviour during wakeful, conscious processing, characterized by a desynchronization of the EEG (Destexhe et al., 1999).

2.6 Acknowledgements

The authors would like to acknowledge the software tools provided by Dr. Kenneth Harris (University College London, UK) for the use of KlustaKwik, and by Dr. A. David Redish (University of Minnesota, Minneapolis, MN) for the use of MClust. We are grateful for the support provided by the technology center of the University of Amsterdam, in particular Gerrit Hardeman, Eric Hennes, Harry Beukers, Ron Manuputy, Matthijs Bakker, Ed de Water, and many others. This work was supported by the Netherlands Organization for Scientific Research-VICI Grant 918.46.609 (to CP) and the EU FP7- ICT grant 270108 (to CP) and from the European Union's Horizon 2020 Framework Programme for Research and Innovation under the Specific Grant Agreement No. 945539 (Human Brain Project SGA3).

2.7 Supplementary data

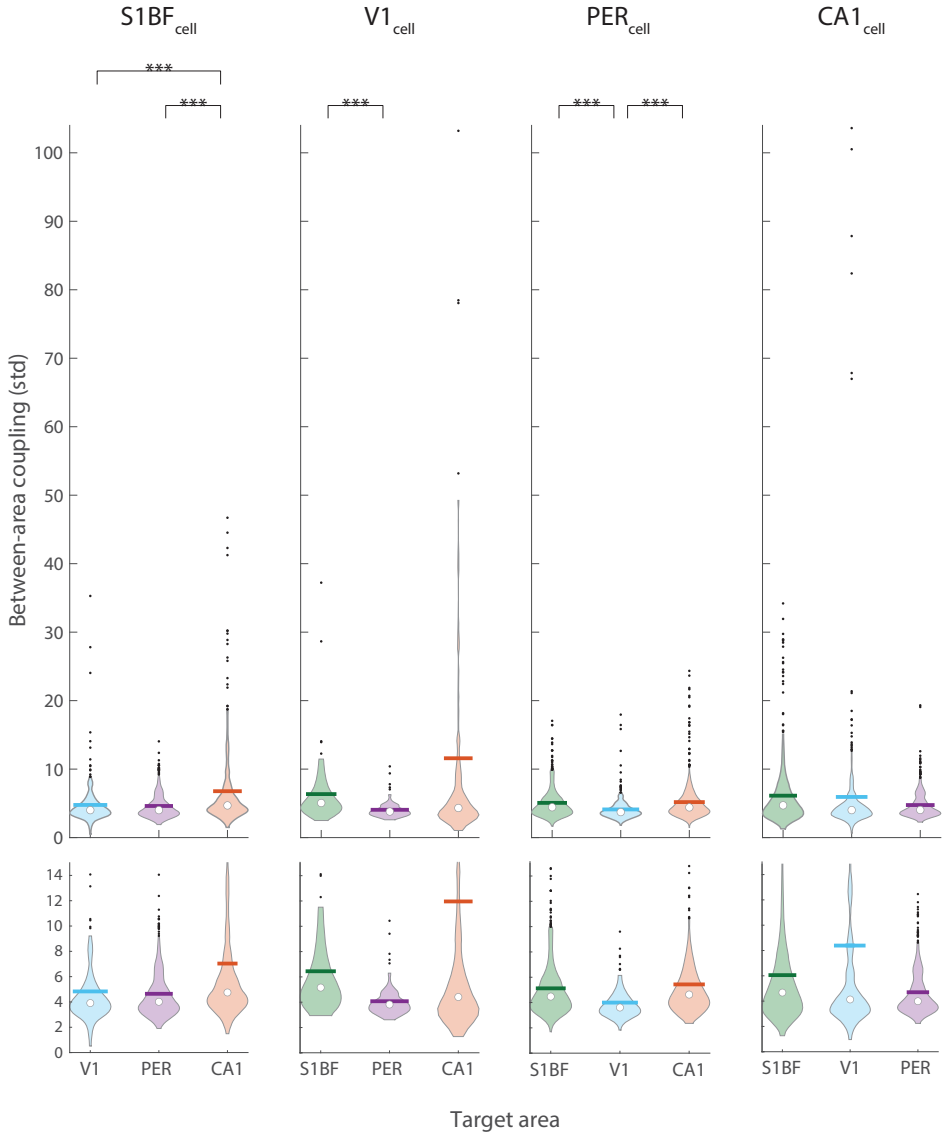

*Figure S1: Between-area coupling relationships specified per reference area. Supplement to figure 3. Violin plots showing spread and averages of between-area coupling values. The four main plots refer to the four reference areas, indicated at the top. The three violins per plot represent the 3 target areas, indicated on the X-axis. Bottom plots are zoomed in on the bodies of the violins to highlight differences. White dot: median, horizontal line: mean, black dots are > 95% percentile outliers. The areas are represented as green (S1BF), blue (V1), violet (PER), orange (CA1). In addition to the between-area coupling profiles as shown in figure 3c, here we aptly see the spread and outliers: sensory cortical cells connecting to CA1, and between sensory areas cells present heavy outliers. ** $p < 0.005$, *** $p < 0.0005$. P-values were Bonferroni corrected for 66 tests. P values of all different combinations are displayed in table 3.*

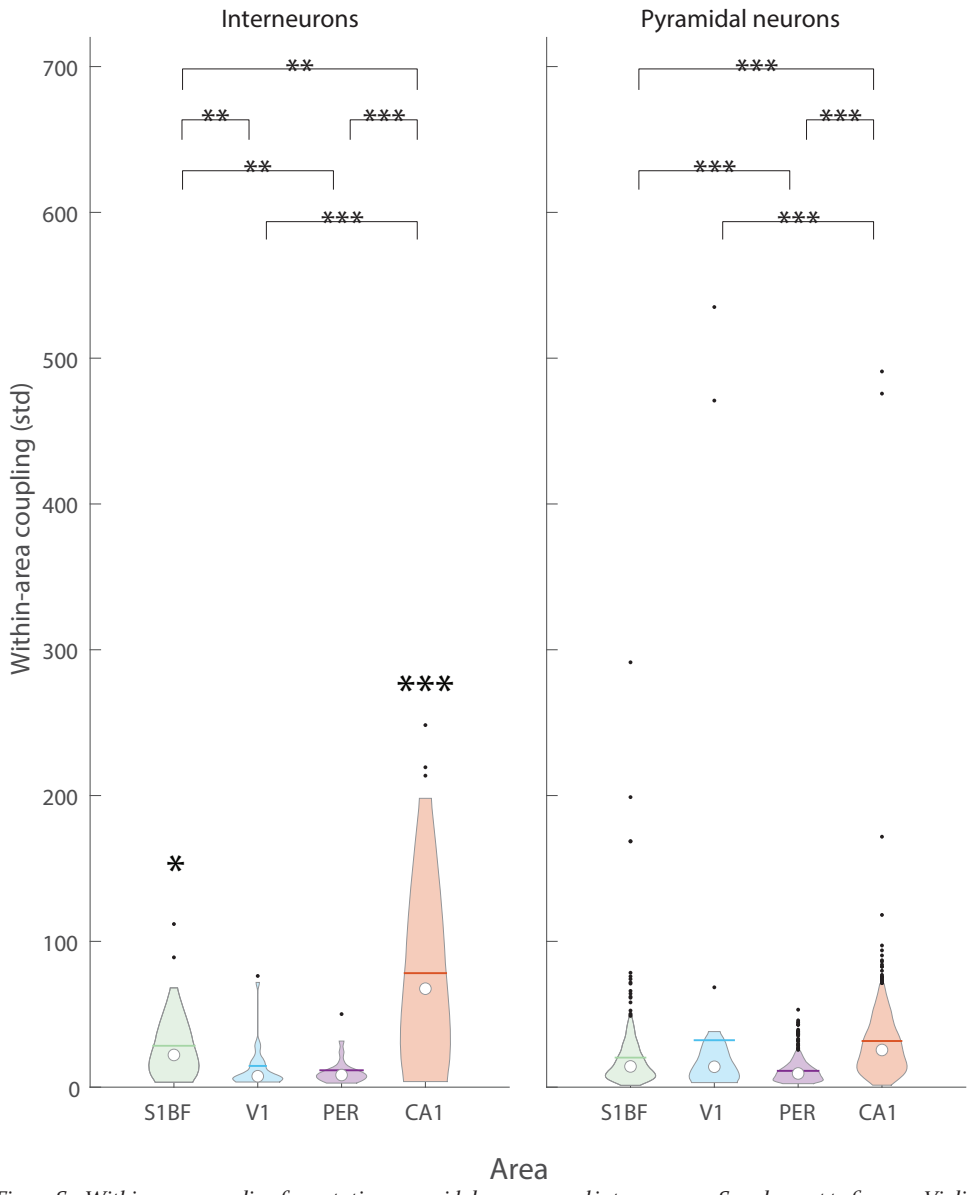

*Figure S2: Within-area coupling for putative pyramidal neurons and interneurons. Supplement to figure 2. Violin plots showing spread and average of within-area population coupling of pyramidal cells and interneurons. Interneurons generally display stronger within-area coupling than pyramidal cells. Relative strengths of within-area coupling are comparable between areas, except for a decreased within-area coupling for inhibitory neurons in visual cortex. White dot: median, horizontal line: mean, black dots are > 95% percentile outliers. The areas are represented as green (S1BF), blue (V1), violet (PER), orange (CA1). Significance lines with asterisks indicate for tests between connections of one cell type. Asterisk above a single violin indicates significant higher coupling compared with the other cell type. ** indicates $p < 0.005$, *** indicates $p < 0.0005$. P-values are Bonferroni-corrected for 12 tests. P values of pyramidal neurons vs interneurons are displayed in table 2.*

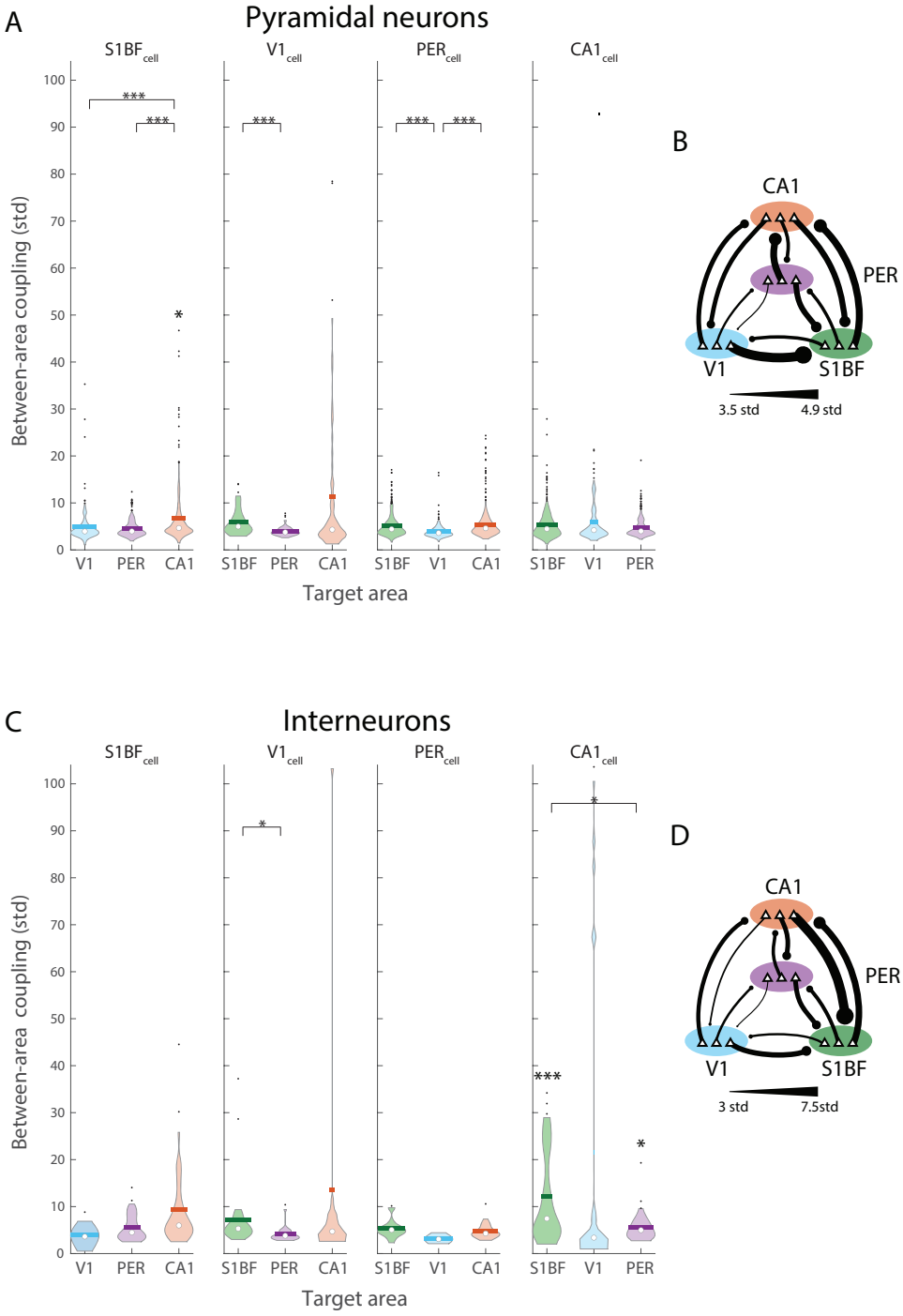
A
Pyramidal neurons
S1BF cell
V1 cell
PER cell
CA1 cell
Between-area coupling (std)
Target area
V1
PER
CA1
S1BF
B
CA1
PER
V1
S1BF
3.5 std
4.9 std
C
Interneurons
D
3 std
7.5std

◀*Figure S3: Between-area coupling for putative interneurons and pyramidal neurons. Supplement to figure 3 and supplementary figure S2. (A) Violin plots showing spread and average of between-area coupling for pyramidal neurons. The four different plots per cell type refer to the four reference areas, indicated at the top. The three violins per plot represent the three target areas, indicated on the x-axis. White dot: median, horizontal line: mean, black dots are > 95% percentile outliers. (B) schematic depiction of the median between-area coupling. Line width depicts median coupling level. (C) Same as A, but for interneurons. Note the smaller amount of interneurons leading to larger variation, and likely affecting significance testing. (D) same as B, but for interneurons. Note the different width scaling between B and D. General patterns appear similar between the two cell types, such as strong coupling between S1BF and CA1, stronger coupling from V1 to S1BF than vice versa, and relatively weak coupling between sensory areas and PER. Significance lines with asterisks indicate for tests between connections of one cell type. The areas are represented as green (S1BF), blue (V1), violet (PER), orange (CA1). Asterisk above a single violin indicates significant higher coupling compared with the other cell type. * indicates $p < 0.05$, *** indicates $p < 0.0005$. P values were Bonferroni corrected for 66 tests. P-values of all different combinations are displayed in table 4, P values of pyramidal neurons vs interneurons are displayed in table 5.*

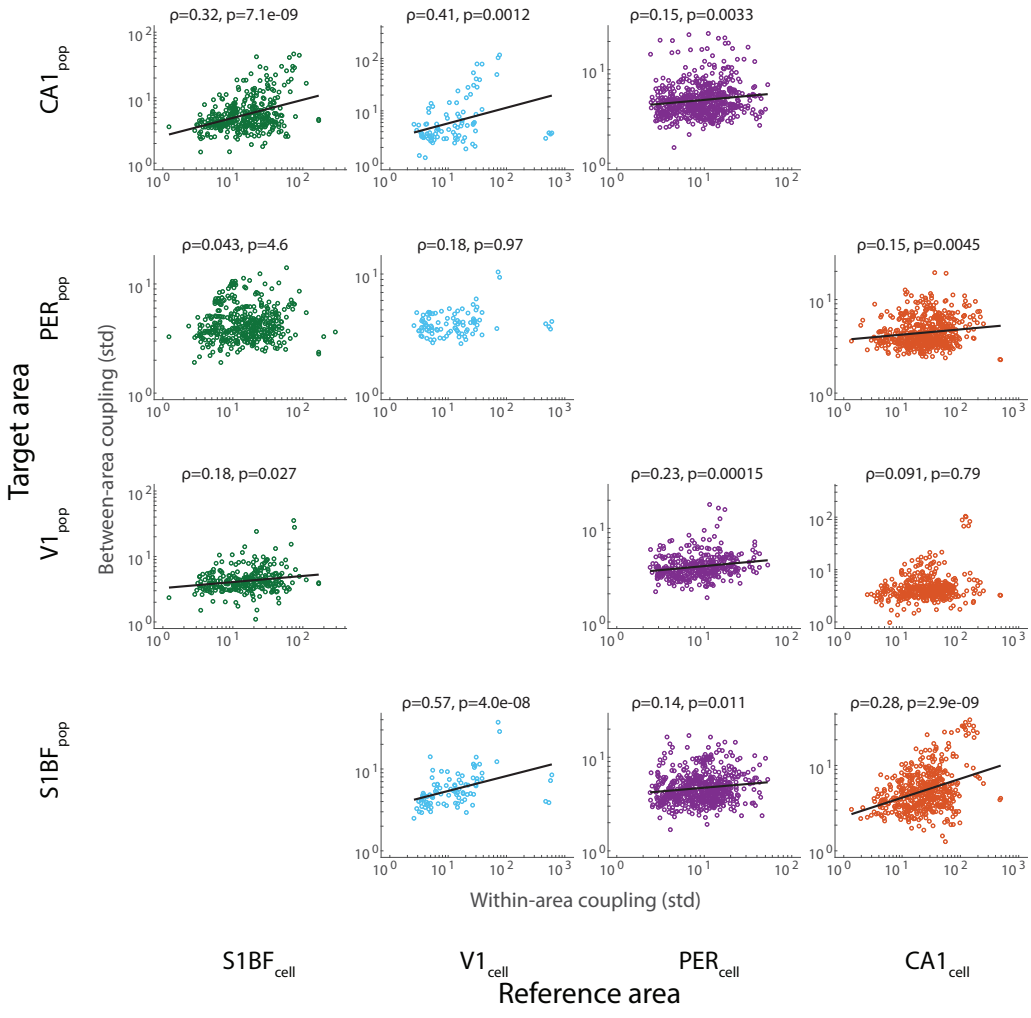

Figure S4: Within- versus between-area coupling for all areas. Supplement to figure 4. Scatterplots of within-area coupling versus between-area coupling, of all four reference areas (columns) and target areas (rows). Overall, weak to moderate, yet significant, positive correlations are selectively found for several pairs of areas. Correlations from and to CA1 appear to consist of a subset of neurons following a positive diagonal trend. Black lines are linear regressions on log-transformed data and are only shown for significant correlations. Correlations are quantified as Spearman's rho. P-values are Bonferroni corrected for 12 tests. Across all images the areas are represented as green (S1BF), blue (V1), violet (PER), orange (CA1) for the appropriate reference area.

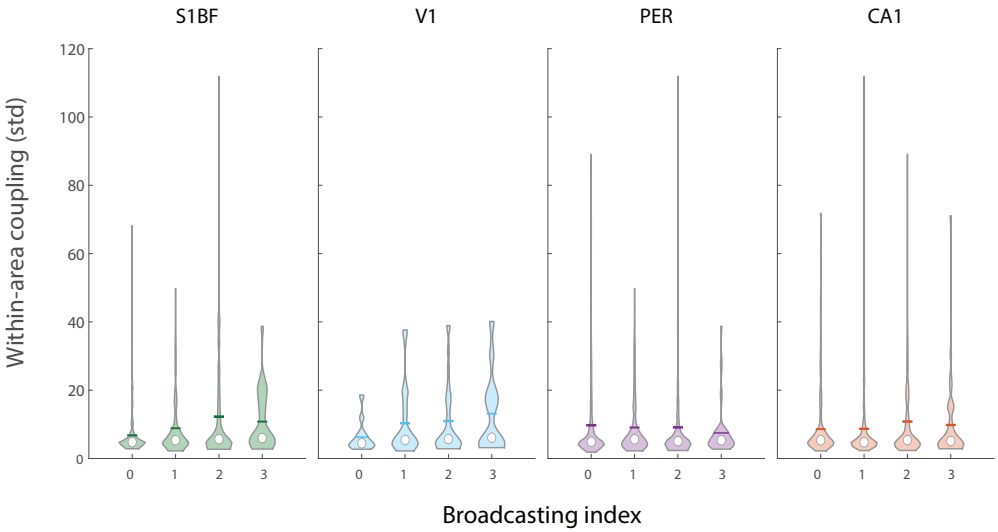

Figure S5: Within-area coupling versus broadcasting indices. Supplement to figure 5. Violin plots of within-area coupling levels per broadcasting index value for the four different areas. Across all graphs the areas are represented as green (S1BF), blue (V1), violet (PER), orange (CA1) for the appropriate area. White dot: median, horizontal line: mean. No significant differences were found between the within-area coupling values as a function of broadcasting index per area.

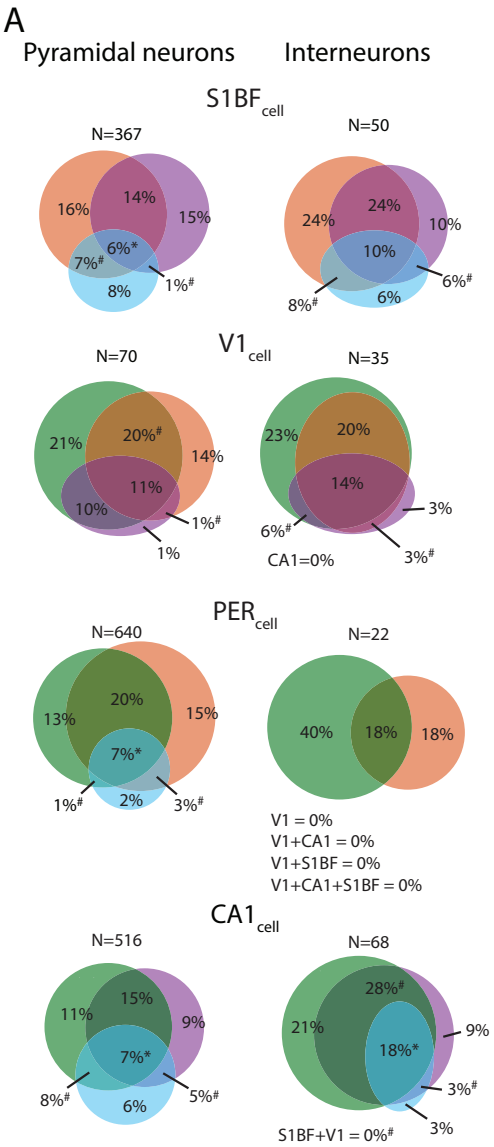
A
Pyramidal neurons
Interneurons
S1BF cell
N=367
16%
14%
15%
6%*
7%#
1%#
8%
N=50
24%
24%
10%
10%
6%#
8%#
6%
V1 cell
N=70
21%
20%#
14%
11%
10%
1%#
1%
N=35
23%
20%
14%
3%
6%#
CA1=0%
3%#
PER cell
N=640
13%
20%
15%
7%*
1%#
2%
3%#
N=22
40%
18%
18%
V1 = 0%
V1+CA1 = 0%
V1+S1BF = 0%
V1+CA1+S1BF = 0%
CA1 cell
N=516
11%
15%
9%
7%*
8%#
6%
5%#
N=68
21%
28%#
18%*
9%
3%#
3%
S1BF+V1 = 0%#

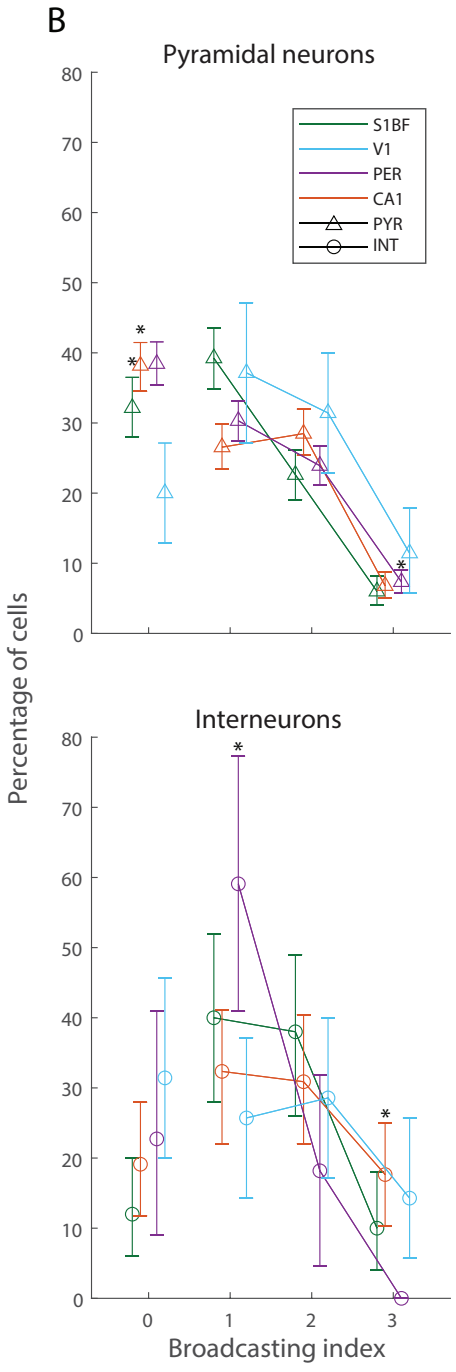
B
Pyramidal neurons
S1BF
V1
PER
CA1
PYR
INT
Interneurons
Percentage of cells
Broadcasting index
0
10
20
30
40
50
60
70
80
1
2
3

◀ *Figure S6: broadcasting indices for interneurons and pyramidal neurons. Supplement to figure 5. (A) Venn diagrams indicating percentages of cells with significant couplings to the various areas. Unconnected areas are noted below the respective diagram. Asterisks and pound symbols show results for bootstrap testing (α = 0.05) if connections to two or more areas are expected compared to the joint probability of cells connecting to one area. Asterisks indicate more cells than expected, and pound symbol less than expected. (B) proportions of cells in a particular area having specified broadcasting indices, for pyramidal neurons (top) and interneurons (bottom). Asterisks above a marker indicates difference between celltype from a bootstrapping test (N = 1000), where the asterisk denotes the significantly higher of the two. Error bars indicate 95% confidence intervals from a bootstrapping procedure. For pyramidal neurons, the general trend remains similar as for the total population (figure 5), while interneurons diverge, but are generally larger than for pyramidal cells. Note the lower number of interneurons, influencing variance. Note PER has no cells with an index = 3. (C) Within area coupling for pyramidal neurons (top) and interneurons (bottom) for all four areas, over different broadcasting indices. The lack of asterisks indicate no significant differences between levels of within-area coupling. Across all images the areas are represented as green (S1BF), blue (V1), violet (PER), orange (CA1) for the appropriate area.*

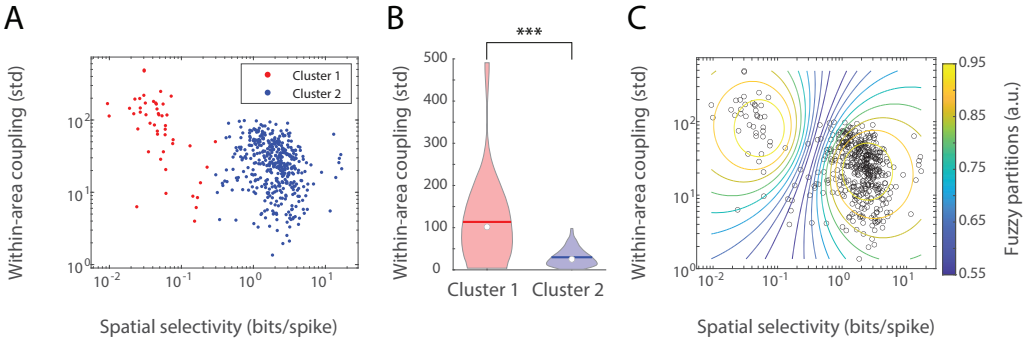

*Figure S7: High spatial selectivity of CA1 cells correlates with low within-area coupling. Supplement to figure 6. (A) Spatial selectivity versus within-area coupling for CA1 neurons, as displayed in figure 6c. Colours indicate two clusters assigned by K-means clustering. Note that not all cells in Cluster 2 (blue) have a spatial selectivity that would qualify them as place cells. (B) Violin plots indicate the difference in within-area coupling between the two clusters. (C) Fuzzy clustering verifies that the clusters are well separated, save for a handful of datapoints between the two clusters. Excluding these ambiguous datapoints (fuzzy partition < 0.75) did not alter the conclusions from this data. Note the logarithmic scale on the scatter plot (A & C), and the linear scale on the violin plots (B). White dot: median, horizontal line: mean. Significance assessed with Wilcoxon's sign-rank test, *** P < 0.0005.*

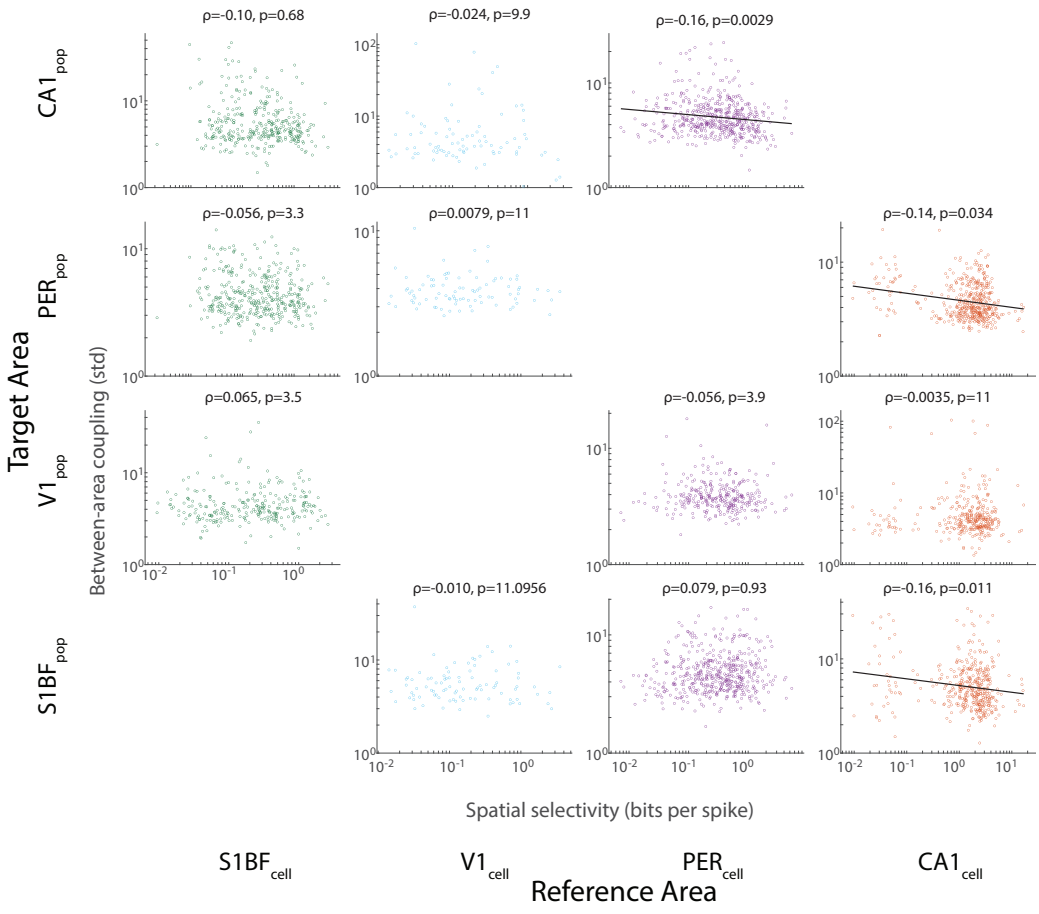

Figure S8: Spatial selectivity versus between-area coupling. Supplement to figure 6. Scatterplots of spatial selectivity versus between-area coupling for all four reference areas (columns) with all target areas (rows). Significant negative correlations are visible in the coupling of CA1 cells with S1BF and PER populations, and in PER cells with CA1 populations. Black lines are linear regressions and are only shown for significant correlations. Correlations are quantified as Spearman's rho. P-values are Bonferroni corrected for 12 tests. Across all graphs the areas are represented as green (S1BF), blue (V1), violet (PER), orange (CA1) for the appropriate reference area.

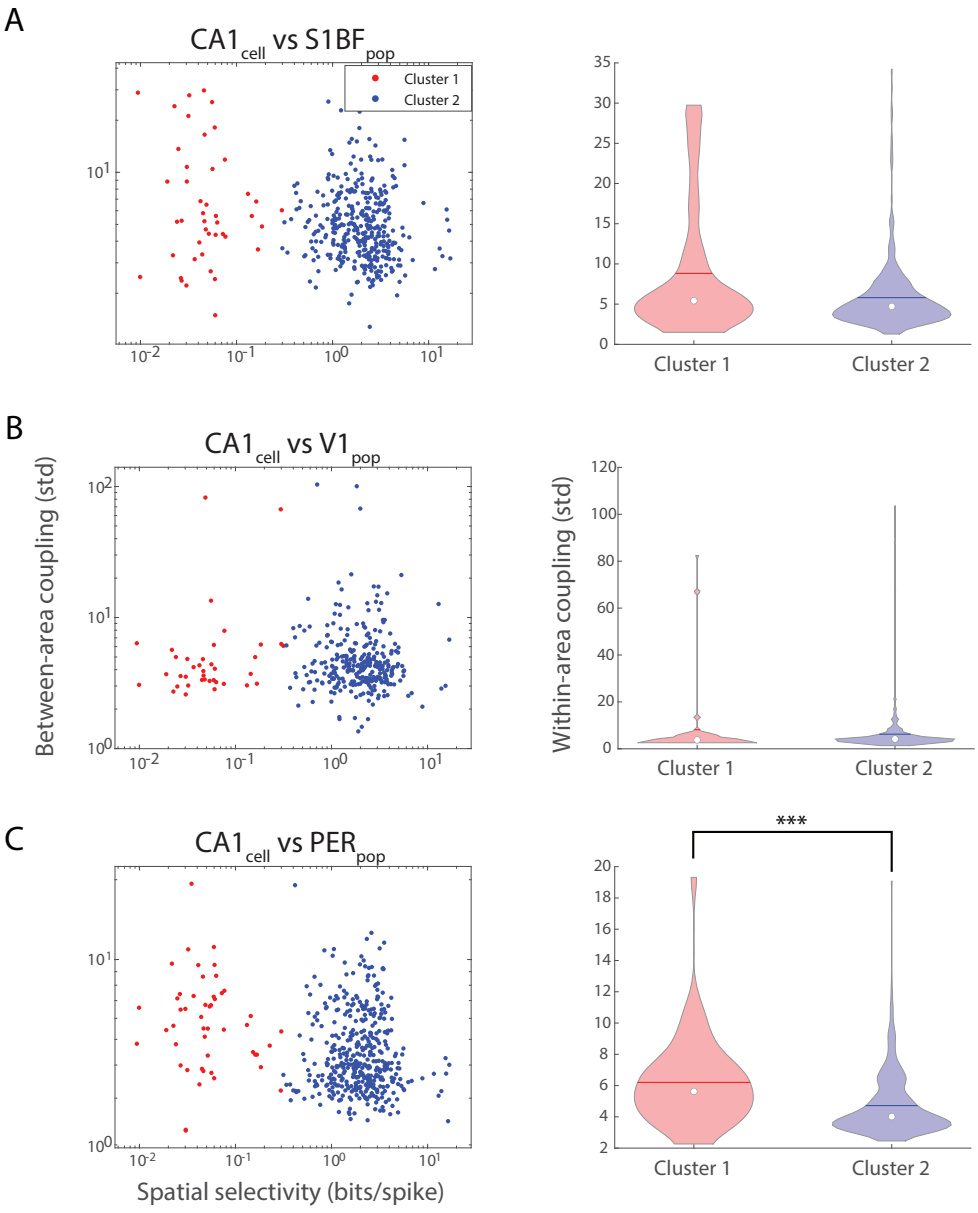

*Figure S9: CA1 spatial selectivity and between-area coupling. Supplement to figure S7 and S8. Spatial selectivity versus between-area coupling for CA1 neurons versus (A) S1BF, (B) V1 and (C) PER. Left column shows scatter plots with colours indicating two clusters assigned by K-means clustering. Right column shows violin plots indicating the difference in between-area coupling between the two clusters. Note the logarithmic scale on the scatter plots (left), and the linear scale on the violin plots (right). Only the coupling of CA1 cells with PER populations was significantly affected by cluster identity. White dot: median, horizontal line: mean. Significance assessed with Wilcoxon's sign-rank test, *** P < 0.005. P values are Bonferroni corrected for 3 tests.*

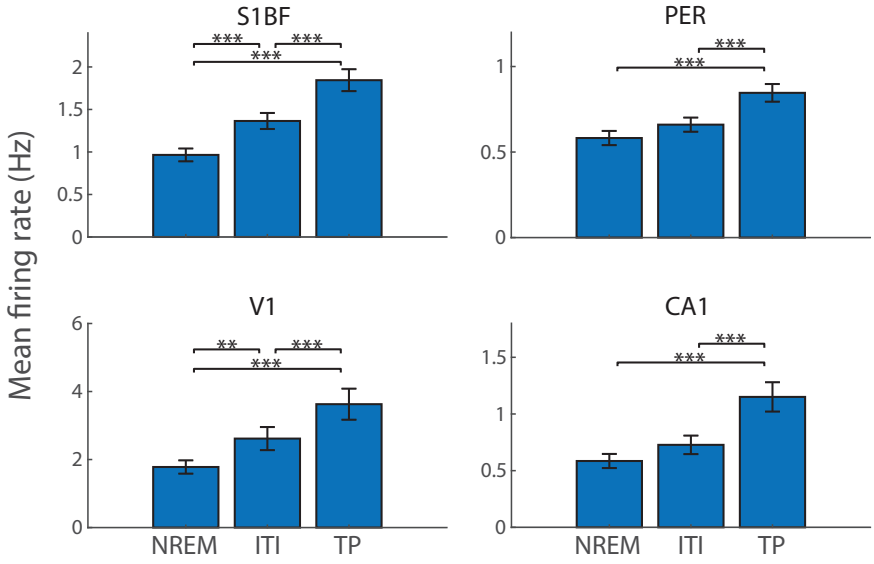

*Figure S10. Mean firing rates for the different areas under varying behavioural conditions. Brain state has a significant effect on mean firing rates in all four areas. NREM: non-REM sleep, ITI: inter-trial interval, TP: task performing epochs. The significance of differences between coupling values in different brain states was assessed with Wilcoxon's sign-rank test, * indicates P < 0.05, ** P < 0.005, *** P < 0.0005. P-values are Bonferroni corrected for 12 tests.*

Figure S11: Between-area coupling during different brain states. Supplement to figure 7. Violin plots of ▶ between-area coupling for three brain states, for all four references areas (columns) with all target areas (rows). Although the changes in coupling across brain states are heterogeneous and depend on the pair of areas, the overall picture is one of gradual changes, not of an overriding state dependence. Noticeable are the declined coupling levels of CA1 neurons with other populations, a tendency of stronger coupling in the TP condition for S1BF populations (although not significant for every reference area), and a lack of change in coupling for V1 cells. White dot: median, horizontal line: mean. The reference areas are represented as green (S1BF), blue (V1), violet (PER), orange (CA1). NREM: non-REM sleep, TP: task performing, ITI: inter-trial interval. Significance was tested by Wilcoxon's sign-rank test, * indicates P < 0.05, ** P < 0.005, *** P < 0.0005. P-values are Bonferroni-corrected for 36 tests.

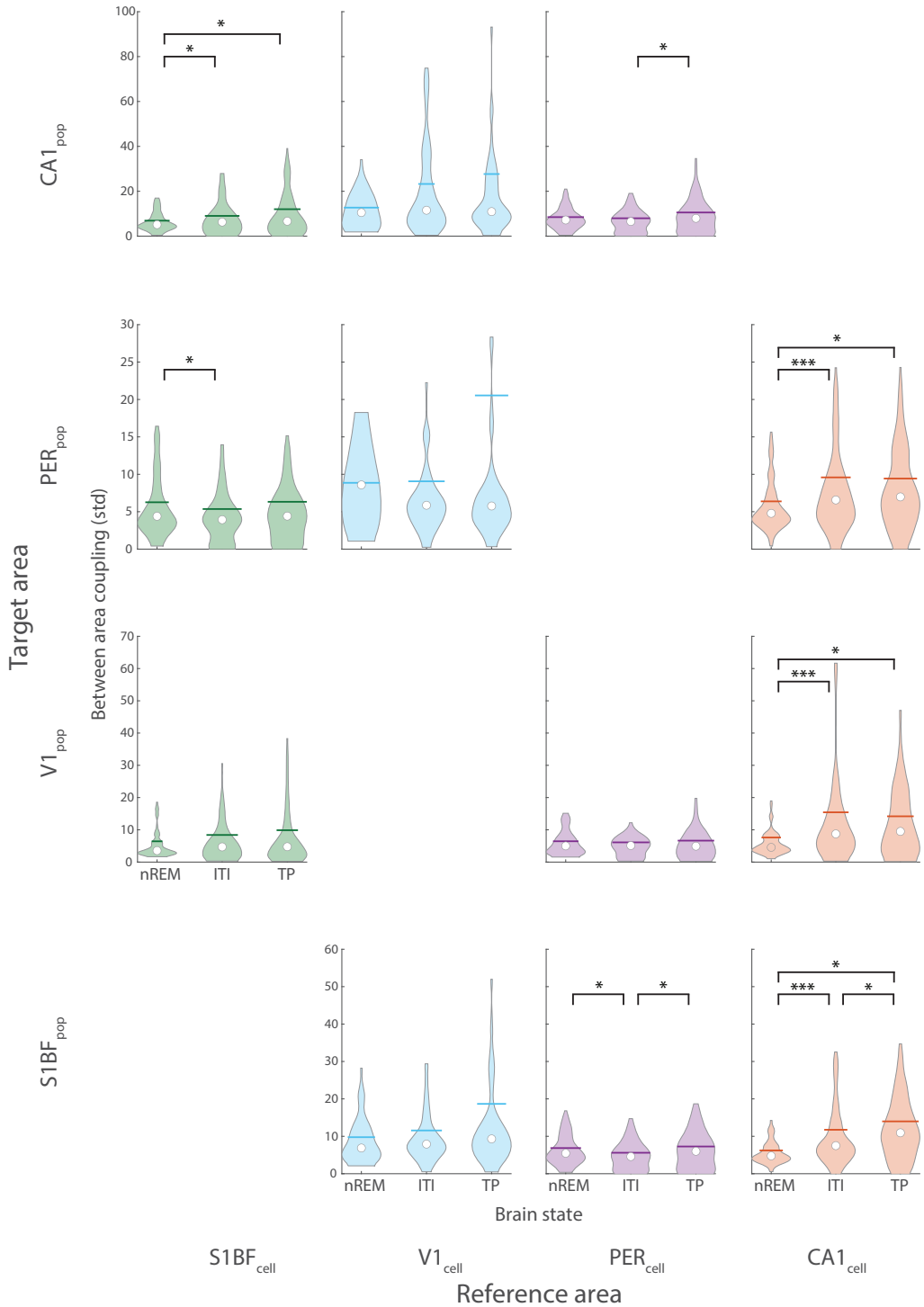
Target area
Between area coupling (std)
CA1pop
PERpop
V1pop
S1BFpop
S1BFcell
V1cell
PERcell
CA1cell
Reference area
nREM
ITI
TP
Brain state
*
***

Reference	Target	Mean	Median	Standard deviation	N	% coupled
S1BF	S1BF	21.21	14.97	24.62	417	93%
	V1	4.83	3.91	3.77	103	33%
	PER	4.64	4.01	1.96	586	39%
	CA1	7.03	4.75	6.43	496	55%
V1	S1BF	6.42	5.13	4.58	278	65%
	V1	26.38	11.64	74.65	96	80%
	PER	4.06	3.80	1.27	368	25%
	CA1	11.86	4.39	20.417	413	49%
PER	S1BF	5.08	4.43	2.28	409	47%
	V1	3.96	3.58	1.66	102	19%
	PER	11.18	9.38	7.96	662	82%
	CA1	5.38	4.59	3.03	577	52%
CA1	S1BF	6.12	4.73	4.76	363	53%
	V1	8.50	4.18	15.58	96	42%
	PER	4.76	4.04	2.01	615	39%
	CA1	37.16	26.86	42.54	583	96%

Table S1: Mean and median coupling values, both within and between areas. The percentage of coupled cells (% coupled) is defined as having a coupling value of 4.5 std or more, for more than 4 ms. Coupling values are Z-scored against a shuffled distribution, meaning this corresponds to 4.5 standard deviations increase from the shuffled distribution (see Methods).

Reference	Target	Mean	Median	Standard deviation	N	% coupled
S1BF	S1BF	-4.71	-3.77	3.21	415	43%
	V1	-3.49	-3.49	0.92	331	32%
	PER	-3.87	-3.65	1.07	391	33%
	CA1	-3.96	-3.65	1.63	183	21%
V1	S1BF	-3.99	-3.71	1.26	101	36%
	V1	-6.03	-4.24	3.91	93	39%
	PER	-3.55	-3.39	0.85	99	25%
	CA1	-4.3	-3.89	1.95	88	53%
PER	S1BF	-4.17	-3.85	1.37	582	43%
	V1	-3.63	-3.4	1.07	520	46%
	PER	-4.36	-3.72	2.38	658	39%
	CA1	-4.42	-3.92	1.85	201	30%
CA1	S1BF	-3.84	-3.62	1.35	492	36%
	V1	-3.9	-3.57	1.47	575	47%
	PER	-3.83	-3.57	1.12	572	34%
	CA1	-4.79	-3.92	3.01	166	34%

Table S2: Mean and median negative coupling values, both within and between areas. The percentage of coupled cells (% coupled) is defined as having a coupling value of 4.5 std or more, for more than 4 ms. Coupling values are Z-scored against a shuffled distribution, meaning this corresponds to 4.5 standard deviations increase from the shuffled distribution (see Methods).

Table 3: Wilcoxon's rank sum test P-values between all area combinations. P-values of Wilcoxon's rank-sum ▶ test of difference between all between-area combinations, complementing figure 3 and S1. Top-left cell provides P-value for the test of difference between $S1BF_{cell}$ - PER_{pop} compared with $S1BF_{cell}$ - $V1_{pop}$. The + and – symbols on significant values indicate whether coupling of a pair in the specific column is larger or smaller, respectively, compared with a pair in the row. Colour coding indicated relevant significance levels: Blue is P < 0.05; Green is P < 0.005; Red is P < 0.0005. All P-values were Bonferroni corrected for 120 tests.

Ref		S1BF		V1			PER			CA1		
	target	PER	CA1	S1BF	PER	CA1	S1BF	V1	CA1	S1BF	V1	PER
S1BF	V1	50.14	+ 2.25E-07	+ 2.53E-06	19.11	4.80	+ 0.027	0.25	+ 0.00032	+ 0.009	14.52	7.41
	PER		+ 5.95E-09	+ 1.56E-06	3.82	7.60	+ 0.036	- 0.00061	+ 0.00012	+ 0.0046	27.73	21.57
	CA1			46.81	- 2.05E-09	23.33	- 0.0034	- 9.05E-20	0.53	2.053	0.17	- 3.11E-08
V1	S1BF				- 2.19E-09	13.64	- 0.0094	- 3.29E-15	0.23	1.48	0.19	- 0.00001
	PER					1.70	+ 0.00014	12.72	+ 5.71E-07	+ 0.00035	3.44	0.14
	CA1						84.48	- 0.02	106.74	107.70	56.7	27.20
PER	S1BF							- 1.12E-13	13.70	18.14	39.13	0.79
	V1								+ 1.44E-17	+ 1.83E-11	+ 0.0085	+ 7.62E-08
	CA1									96.20	9.12	- 0.0028
CA1	S1BF										24.8	0.067
	V1											87.08

Area	P-value
S1BF	0.015
V1	1.038
PER	2.20
CA1	4.11E-07

Table S4: Within-area coupling: interneurons versus pyramidal cells. P-values of Wilcoxon's rank-sum test of difference between within-area coupling for pyramidal neurons and interneurons, complementing figure S2. P-values were Bonferroni corrected for 4 tests.

		Target area			
		S1BF	**V1**	**PER**	**CA1**
Ref area	**S1BF**		5.43	0.47	+ 0.046
	V1	7.77		11.44	9.57
	PER	1.63	0.87		7.86
	CA1	- 7.24E-07	1.46	+ 0.020	

Table 6: Between-area coupling, Interneurons versus pyramidal cells. P-values of Wilcoxon's rank-sum test of difference between between-area coupling for pyramidal neurons and interneurons, complementing figure S2. P-values were Bonferroni corrected for 12 tests. The + and – symbol on significant values indicate if pyramidal cells have higher or lower coupling, respectively. Colour coding indicates relevant significance levels: Blue is P < 0.05; Green is P < 0.005; Red is P < 0.0005. All P-values were Bonferroni corrected for 120 tests.

Pyramidals

Ref	target	S1BF		V1			PER			CA1		
		PER	CA1	S1BF	PER	CA1	S1BF	V1	CA1	S1BF	V1	PER
S1BF	V1	99.26	+ 4.02E-05	+ 0.00090	19.83	17.87	0.12	0.31	+ 0.00097	0.72	6.98	32.45
	PER		+ 1.88E-07	+ 0.00013	13.0	15.76	+ 0.010	- 0.014	+ 8.30E-06	0.11	4.08	27.89
	CA1			41.17	- 3.50E-06	44.62	0.11	- 4.35E-16	8.78	0.75	3.01	- 6.57E-07
V1	S1BF				- 8.92E-06	30.41	0.22	- 6.42E-10	3.079	0.97	2.25	- 0.00063
	PER					11.15	+ 0.0047	21.93	+ 3.39E-05	0.054	1.40	2.012
	CA1						101.61	0.66	94.52	69.67	102.24	42.06
PER	S1BF							- 5.72E-12	8.48	114.05	94.29	0.15
	V1								+ 3.23E-16	+ 9.27E-08	+ 0.00095	+ 1.59E-05
	CA1									25.41	26.75	- 9.24E-05
CA1	S1BF										101.82	1.30
	V1											20.99

Interneurons

Ref	target	S1BF		V1			PER			CA1		
		PER	CA1	S1BF	PER	CA1	S1BF	V1	CA1	S1BF	V1	PER
S1BF	V1	11.15	0.20	1.29	98.83	14.9	7.52	47.71	26.97	0.050	83.25	5.57
	PER		1.37	20.29	6.38	109.08	60.61	0.96	97.95	+ 0.036	14.79	82.97
	CA1			20.65	- 0.0050	6.83	6.04	0.095	1.17	33.74	2.54	1.13
V1	S1BF				- 0.010	31.93	55.38	0.067	6.045	5.12	5.50	31.28
	PER					7.31	0.31	7.23	5.15	- 0.00041	56.47	0.34
	CA1						79.10	1.66	88.81	2.093	17.14	93.45
PER	S1BF							0.29	26.75	1.52	13.70	106.91
	V1								0.79	0.070	59.46	0.22
	CA1									0.31	27.39	41.86
CA1	S1BF										1.31	- 0.035
	V1											7.77

◀ *Table S5: Wilcoxon's rank sum test P-values between all area-area combinations for putative pyramidal cells and interneurons. P-values of Wilcoxon's rank-sum test of difference between all between-area combinations for only putative pyramidal (top) or interneurons (bottom), complementing figure S3. Same conventions as Table 3. The + and – symbols on significant values indicate whether coupling of a pair in the specific column is larger or smaller, respectively, compared with a pair in the row. Colour coding indicated relevant significance levels: Blue is P < 0.05; Green is P < 0.005; Red is P < 0.0005. All P-values were Bonferroni corrected for 120 tests.*